



THE HONG KONG
POLYTECHNIC UNIVERSITY

香港理工大學

Pao Yue-kong Library

包玉剛圖書館

Copyright Undertaking

This thesis is protected by copyright, with all rights reserved.

By reading and using the thesis, the reader understands and agrees to the following terms:

1. The reader will abide by the rules and legal ordinances governing copyright regarding the use of the thesis.
2. The reader will use the thesis for the purpose of research or private study only and not for distribution or further reproduction or any other purpose.
3. The reader agrees to indemnify and hold the University harmless from and against any loss, damage, cost, liability or expenses arising from copyright infringement or unauthorized usage.

If you have reasons to believe that any materials in this thesis are deemed not suitable to be distributed in this form, or a copyright owner having difficulty with the material being included in our database, please contact lbsys@polyu.edu.hk providing details. The Library will look into your claim and consider taking remedial action upon receipt of the written requests.

**A Proton Exchange Membrane Fuel Cell
(PEMFC) Model
for Use in Power Electronics**

Jerome, Ho-Chun LEE

*Department of Electronic and Information Engineering,
The Hong Kong Polytechnic University, Hung Hom, Hong Kong.*

Thesis Submitted for
the Degree of Master of Philosophy

March 2005



Pao Yue-kong Library
PolyU · Hong Kong

Certificate of originality

I hereby declare that this thesis is my own work and that, to the best of my knowledge and belief, it reproduces no material previously published or written nor material which has been accepted for the award of any other degree or diploma, except where due acknowledgment has been made in the text.

_____ (Signed)

Jerome, Ho-Chun LEE _____ (Name of student)

To my parents

Abstract

Abstract of the thesis entitled 'A Proton Exchange Membrane Fuel Cell (PEMFC) Model for Use in Power Electronics' submitted by Jerome Ho-Chun LEE for the degree of Master of Philosophy at The Hong Kong Polytechnic University in June 2004

Fuel cell is considered as the most environmentally green energy source. Electricity is generated by the reaction of hydrogen and oxygen with the byproduct of water. This technology has been adopted in space programs since 1968. However, due to the high cost in material and system complexity, this technology has not been widely used in public. Recently, as a result of the support from the US government and the influence of energy crises, fuel cells are now gaining attention in the public and research programs. A number of remarkable advancements, including the creation of polymer membrane, reduction in

platinum content and invention of hydrogen reformer, enable fuel cells to get closer to the general public. Still, a number of weaknesses, such as instability of output power, long startup time, slow dynamic responses and complexity in system design are impeding the progress of fuel cell development. These issues are still challenges to power electronics engineers. Novel approaches such as application of bi-directional conversion, assistance of super capacitor and integration of hybrid system etc. are proposed to solve some problems. Unfortunately, engineers have been slow in considering the relationship between fuel cell and power manipulation system. A fuel cell has a very unstable voltage which is sensitive to fuel purity, operation pressure, temperature and hydration. As a result, separate system considerations cannot lead to satisfactory results in term of overall system efficiency, stability and usability. The objective of this study is to fill this gap by presenting the operation of fuel cell system in an understandable language to electronic engineers. In addition, a proton exchange membrane fuel cell (PEMFC) model was proposed in this thesis. The model was then integrated into a PSpice simulator. By doing so, it is expected that electronic engineers can have a more in depth understanding of the fuel cell operation. The objective is to create a more reliable system with higher efficiency. Detailed simulation results based on MathCAD and PSpice are given. Suggestions and comparisons are also provided in this thesis.

Acknowledgements

I would like to take this opportunity to express my sincere gratitude to my Chief Supervisor, Prof. Y. S. Lee, for his encouragement and guidance throughout the course of this research study. His immense enthusiasm for research is greatly appreciated. Both his professional advice and plentiful experience help me to further improve myself.

I would also like to express my gratitude to Dr. H. L. Chow and Prof. D. Sultanto, my co-supervisors, for their support and constructive comments, that will never be forgotten. Their expert knowledge and friendly encouragement have helped me to overcome a lot of difficulties during my study.

I would also like to thank Dr. W.S. Li, for his helpful suggestions and patient guidance. In addition, I should not forget to thank Mr. C. P. Lee and Dr. E. Jelenkovic, for their kind assistance in performing the experimental tests. I

will be forever grateful to my colleagues who have imparted direct assistance on me during the course of my study. In particular, I would like to convey my heartfelt thanks to Dr. L. K. Wong, Dr. K. W. Siu, Dr. W. K. Ling, and Mr. L. P. Wong for their incessant support and inspiration. It has been a very enjoyable experience working with them.

I gratefully acknowledge the Research Committee of The Hong Kong Polytechnic University for its financial support during the entire period of my candidature.

Finally, I must thank my parents, my sister and Vivian for their never-ending support and encouragement. Without their backing, this study would not have the chance to be completed.

Contents

Abstract	ii
1 Introduction	2
1.1 Fuel cell in general	2
1.2 Motivation	3
1.3 Organization of the thesis	4
2 Fundamental of fuel cell	6
2.1 The birth of fuel cell	7
2.2 Fundamental of fuel cell operation	9
2.3 Environmentally green energy source	12
2.4 Types of fuel cells	15
2.5 Structure of Proton Exchange Membrane Fuel Cell (PEMFC)	19
2.5.1 Membrane	19
2.5.1.1 Recent advancement	21

2.5.2	Electrodes and electrocatalyst	22
2.5.3	Membrane Electrode Assembly (MEA)	25
2.5.3.1	Recent advancement	27
2.5.4	Bi-polar plate	28
2.5.4.1	Recent advancement	30
2.6	Filling issue	31
2.6.0.2	Pressurized hydrogen	31
2.6.0.3	Liquid hydrogen (LH ₂)	32
2.6.0.4	Reversible Metal Hydride Storage	33
2.6.0.5	Hydrogen reformer	34
3	Proton exchange membrane fuel cell system	36
3.1	Introduction	36
3.2	Fuel processor (Reformer)	38
3.3	Air management sub-system	39
3.4	Water management sub-system	40
3.5	Thermal management sub-system	41
3.6	Power conditioner	42
3.6.1	DC regulation	43
3.6.2	AC conversion	43
4	Model of PEMFC system	44

4.1	Loading characteristic	45
4.2	Reactants flow rate	48
4.3	Water management sub-system	50
4.3.1	Water activity	50
4.4	Proton conductivity in membrane	54
4.5	Thermal management sub-system	55
4.6	Elaboration on the PEMFC Model	58
4.6.1	Initialization mode	67
4.6.2	Standby mode	69
4.6.3	Boost mode	70
5	Modeling and Simulation Using PSpice	72
5.1	Analogue behavior model	73
5.2	Preliminaries	73
5.3	Spice Model	74
5.4	Voltage losses in PEMFC operation	78
5.4.1	Voltage loss due to membrane hydration	78
5.4.1.1	ABM - <i>Net_water</i>	78
5.4.1.2	ABM - <i>Sat_water_P</i>	79
5.4.1.3	ABM - <i>Net_water_act</i>	80
5.4.1.4	ABM - <i>Lamda</i>	80

5.4.1.5	ABM - <i>Vdrop_mem_hyd</i>	80
5.4.2	Voltage loss due to mass transfer	81
5.4.3	Voltage loss due to activation	82
5.4.3.1	ABM - <i>Vdrop_act</i>	82
5.4.4	Voltage loss due to ohmic	82
5.4.4.1	ABM - <i>Int_res</i>	82
5.4.4.2	ABM - <i>Vdrop_In_res</i>	83
5.5	Fuel cell output terminal	83
5.6	Reactants Usage	84
5.6.0.3	ABM - <i>O2_required</i>	84
5.6.0.4	ABM - <i>Air_required</i>	84
5.6.0.5	ABM - <i>Air_required_kgs</i>	85
5.6.0.6	ABM - <i>H2_required</i>	85
5.7	Simulation results	86
5.7.1	Voltage versus current characteristic	86
5.7.2	Fuel cell operation characteristics	88
5.7.3	Fuel usage	92
5.7.4	Application of the PSpice model in UPS system	95
5.8	Conclusion	96
6	Evaluation of Model	98

6.1	Voltage Characteristic	98
6.2	Pressurization effect	102
6.3	Stoichiometric Rate Effect	105
6.4	Startup delay	109
7	Conclusion	112
7.1	Summary of original result	112
7.2	Further Extension	114
7.2.1	Improving accuracy in modeling mass transfer effect . . .	114
7.2.2	System optimization	115
7.2.3	Laplace Sources	116
	Appendix	117
A.1	.cir simulation file for PSpice	117
A.2	MathCad simulation	119
	Bibliography	124

List of Figures

2.1	Conversion of energy in fuel cell.	6
2.2	An illustration of Grove's Experiment of 1839.[1]	10
2.3	Basic construction of a hydrogen fuel cell	11
2.4	Partition of green house gases in ambient	13
2.5	The structure of Nafion 117 from Dupont.	20
2.6	An illustration of a single PEMFC electrode structure and catalyst arrangement.	23
2.7	A commercialized Membrane Electrode Assembly (MEA).	26
2.8	An illustration of bi-polar plate on cathode side.	29
2.9	An illustration of bi-polar plate on anode side.	29
2.10	Metal hydride container.	34
3.1	A Completed PEMFC System	37
4.1	Saturated vapor pressure	53

4.2	Effect of temperature: Cell potential against current density plot with inlet pressure at 2 atm and stoichiometric rate set at 2.	59
4.3	Overpotentials due to temperature at 100°C.	60
4.4	Effect of Cell potential against current density plot with PEMFC temperature kept at 70°C and stoichiometric rate set at 2.	62
4.5	Percentage of energy used by the compressor with respect to the PEMFC electrical output.	63
4.6	Effect of stoichiometric rate: Cell potential against current density plot with inlet pressure at 2 atm and PEMFC temperature kept at 70°C.	64
4.7	A quantitative illustration of the startup delay. Current density at 0.5A/cm ² and cell temperature at 70°C.	68
5.1	An illustration of PEMFC system model in PSpice.	76
5.2	Illustration of the sub-functional block - voltage loss due to membrane conductivity in PSpice.	79
5.3	Illustration of fuel consumption in PSpice.	84
5.4	A typical voltage versus current characteristic of a PEMFC in PSpice simulation with pressure in cathode = 1 bar, operation temperature at 60 °C and stoichiometric rate = 2.	87

5.5	Effect on pressurization in PSpice simulation with temperature at 60 °C and stoichiometric rate = 2. Pressure at cathode = 0.5 bar (□), 1 bar (◇), 2 bar (▽), 3 bar (△), 4 bar (◇) and 5 bar (+).	89
5.6	Effect on stoichiometric rate effect in PSpice simulation with operation temperature at 60 °C and cathode pressure = 1 bar. Stoichiometric rate = 0.1 (□), 1 (◇), 2 (▽), 3 (), 4 (◇), 5 (+) and 6 (×)	90
5.7	Startup effect in PSpice simulation with operation temperature at 60 °C, cathode pressure = 1 bar with current consumption of 0.2A/cm ² . Stoichiometric rate = 1, 2, 3, 4, 5, 6 and 7.	91
5.8	Air consumption (liter/minute) in PSpice simulation with operation temperature at 60 °C, cathode pressure = 1 bar and stoichiometric rate = 2. X-axis indicates current density in A/cm ² , Y-axis indicates flow rate of air in liter/min.	93
5.9	Hydrogen consumption in PSpice simulation with operation temperature at 60 °C, cathode pressure = 1 bar and stoichiometric rate = 2. X-axis indicates current density in A/cm ² , Y-axis indicates flow rate of hydrogen in liter/min.	94

6.1	Voltage against current characteristics in PSpice simulation with operation temperature at 60°C, cathode pressure = 1 bar and stoichiometric rate = 2.	100
6.2	Experimental result of voltage against current characteristics with cathode pressure = 1 bar and air flow of 0.8L/min.	101
6.3	Experimental result on pressurization with stoichiometric rate = 2. Pressure at cathode = 0.5 bar, 1 bar, 2 bar, 3 bar, 4 bar and 5 bar.	103
6.4	Effect on pressurization in PSpice simulation with temperature at 60 °C and stoichiometric rate = 2. Pressure at cathode = 0.5 bar (□), 1 bar (◇), 2 bar (▽), 3 bar (△), 4 bar (◊) and 5 bar (+).	104
6.5	Effect on stoichiometric rate in PSPICE simulation with operation temperature at 60 °C and cathode pressure = 1 bar. Stoichiometric rate = 0.1 (□), 1 (◇), 2 (▽), 3 (), 4 (◊), 5 (+) and 6 (×)	105
6.6	Experimental result on stoichiometric rate with cathode pressure = 1 bar. Air flow in cathode = 0.1L/min, 0.2L/min, 0.3L/min, 0.4L/min, 0.5L/min, 0.6L/min, 0.7L/min, 0.8L/min, 0.9L/min and 1L/min	106
6.7	Experimental startup delay	110

6.8	Startup delay of PEMFC in PSpice simulation	111
A.1	MatCAD Simulation	120

List of Tables

2.1	Comparison between existing technologies	14
2.2	Types of fuel cells	16
2.3	Characteristic of pressurized system	32
2.4	Characteristic of liquified hydrogen system	33
2.5	Characteristic of metal hydride system	35
4.1	Parameter for simulation	57
4.2	Summary of suggested operation mode.	66
5.1	Summary of AMBs and its relationship with electrochemical model	77

Chapter 1

Introduction

1.1 Fuel cell in general

Fuel cell is a chemical device that generates electricity by combining hydrogen and oxygen. Unlike conventional energy sources, in fuel cell, energy is directly extracted from chemical fuels without combustion and auxiliary processing. Thus, fuel cells can provide higher energy conversion efficiency.

Due to the complexity of the system and high capital cost, fuel cells for domestic use are still rarely seen. However, due to the growing concern on the environment and the issue of energy crisis, people start looking for alternative sources of energy. Fuel cell, thus, becomes one of the most promising candidate.

Even though the technology of fuel cell has been developed for more than 60 years, this technology is not seriously taken into consideration until recent years. This thesis is specifically focused on the proton exchange membrane fuel cell (PEMFC) and its application in power electronics. It covers the fundamental technology of fuel cell. In addition, materials are all developed based on the issues of power electronics.

1.2 Motivation

Fuel cell cannot be a standalone product. In the energy transformation process, fuel cell requires peripheral devices to sustain its operation. The overall system performance highly depends on the cooperation of peripheral devices, while each of them possesses its own characteristics. Thus, the difficulties in system integration is relatively greater in fuel cell systems. In practice, each system component can be tuned manually to obtain a reasonable result within a period of time, however, this also introduces overhead and lowers the overall system efficiency. One of the typical example is the fuel pressure. By increasing the pressure of the inlet fuels, higher fuel cell voltage can be obtained. Yet, the energy used in pressurization may not be compensated from a system point of view. In addition, one of the most critical issues, the slow transient response

of the fuel cell, must be carefully considered . All in all, the system is highly complex and involves multi-disciplines.

Existing literatures are mostly focused on the individual components of the fuel cell. Few of them consider all things at the same time. The aim of this thesis is mainly to carry out a systematic investigation on fuel cell from the electronic engineer's point of view. In fact, intensive research and development have been done on chemistry and material science to enable fuel cell to get close to domestic application. On the contrary, little activity has been done on the related power electronics discipline. As a matter of fact, different from conventional portable energy sources, special attention is required in fuel cell operation. This thesis will cover the crucial element in electrochemistry in a language understandable to electronic engineers. It aims at providing a linkage between electrochemistry and electronics, so that power electronics designers can have more in depth understanding in the overall system consideration.

1.3 Organization of the thesis

Chapter 2 will introduce the fundamental theory of fuel cell operation. It introduces various kinds of fuel cells and their characteristics. Regarding proton exchange membrane fuel cell (PEMFC), more in depth review is provided based on existing technology.

Chapter 3 focuses on a PEMFC system. It covers the necessary sub-systems in a PEMFC system. The function of each sub-system will be covered in this chapter.

In Chapter 4, a model with regard to the PEMFC system described in Chapter 3 will be developed. In addition, based on the model, an elaboration on the characteristics of the system will be given in this chapter.

In Chapter 5, a PSpice model of the PEMFC system will be developed. Detailed simulation results will also be presented.

In Chapter 6, an evaluation of the model will be given. Since an intensive amount of dynamics are involved in PEMFC system. This chapter will focus on the attention required with regard to the application of the model. Both strengths and weakness of the model will be pointed out in this chapter for a reference.

A conclusion will be given in Chapter 7, which includes the significance of the work done. In addition, suggestion and improvement will also be presented in this chapter.

Chapter 2

Fundamental of fuel cell

Fossil fuels and its affiliates have been widely used for many years. Until recent years, hydrogen fuel cells, especially the proton exchange membrane fuel cell, demonstrate promising results in stationary and portable applications.

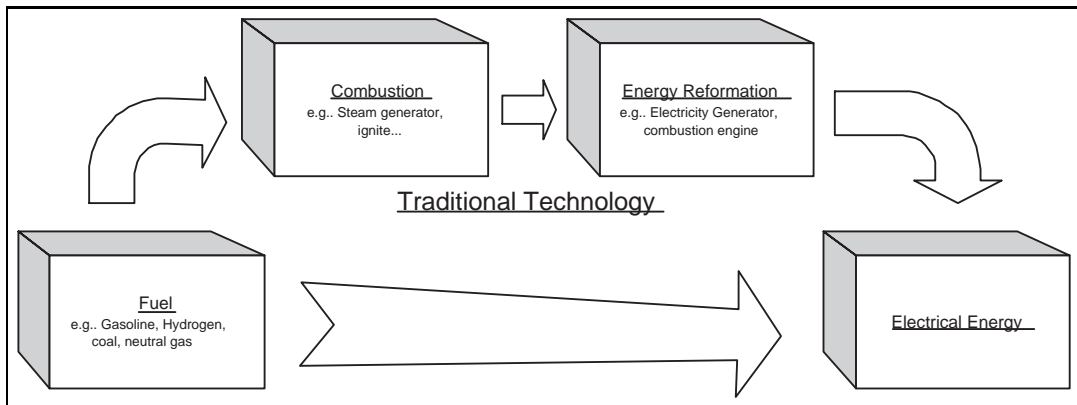


Figure 2.1: Conversion of energy in fuel cell.

As seen in Figure 2.1, a fuel cell is a chemical device that generates electricity by combining hydrogen and oxygen. This form of energy source is significantly different from the traditional ones. In a fuel cell system, electricity is directly generated from hydrogen without pre-processing. As a result, it has a higher energy conversion efficiency.

2.1 The birth of fuel cell

Fuel cell was invented by Sir Grove William in 1839. He reported that voltage had been observed in his laboratory during the combination of hydrogen and oxygen in a galvanic cell by the use of platinum electrodes[1]. The electromotive force of the “Grove Cell” was remarkable for those days: 1.8V - 2.0V. From that time on, Grove William is regarded as the inventor of hydrogen fuel cell. Grove’s first useful fuel cell was seen in 1845 [2].

In the following 50 years, F.T. Bacon, O.K. Davtyan and E.E. Justi continued research activities that put fuel cell into technological development. In 1961, an industrial firm, Energy Conversion, with F.T.Bacon as a consultant worked together with another firm, Pratt & Whitney, to develop a fuel cell for Apollo mission.

In 1968, an alkali fuel cell system developed by F.T. Bacon, was first used in the NASA mission which enabled the “man in the moon” program. This technology was then dominated only in space programs for nearly 20 years. In 1993, California Environmental Legislations and the USA Partnership for a New Generation of Vehicles (PNGV) was launched in California. The program was supported and sponsored by US government. Under this program, all running vehicles have to be fuel economical up to three times (80 miles per gallon) that of comparable 1994 family sedans. Meanwhile, these vehicles must be comparable in terms of performance, size and emissions requirements. The advocacy of PNGV, in turn, gave birth to the R&D programs. Consequently, fuel cell, the ideally green energy source, starts drawing its attention in the public.

Nowadays, major car manufacturers, such as Toyota, Honda, Daimler Chrysler, Ford etc. have already made demonstration vehicles driven by fuel cells. It is believed that the fuel cell will be a promising energy source in the future.

2.2 Fundamental of fuel cell operation

The principle of operation of fuel cell is simple. As shown in the middle of Figure 2.2, when a battery is connected to the platinum electrodes, electric current flow through the water. Water is being electrolyzed. Oxygen and hydrogen are generated on the cathode and anode respectively, and collected by the tubes. On the rightmost figure, when the battery is then replaced by an ammeter, a current is observed flowing through the circuit. The fuel cell operation can be described by the chemical reaction Eq. 2.1.



However, in the arrangement shown in Figure 2.2, the contact area between the electrode and the electrolyte is small.

Figure 2.3 shows the structure of a more advanced version of fuel cell structure. Here, hydrogen is first decomposed into ions. The H^+ ions then pass through the electrolyte to reach the cathode. Meanwhile, electronic is flowing through the external circuit and generating a current.

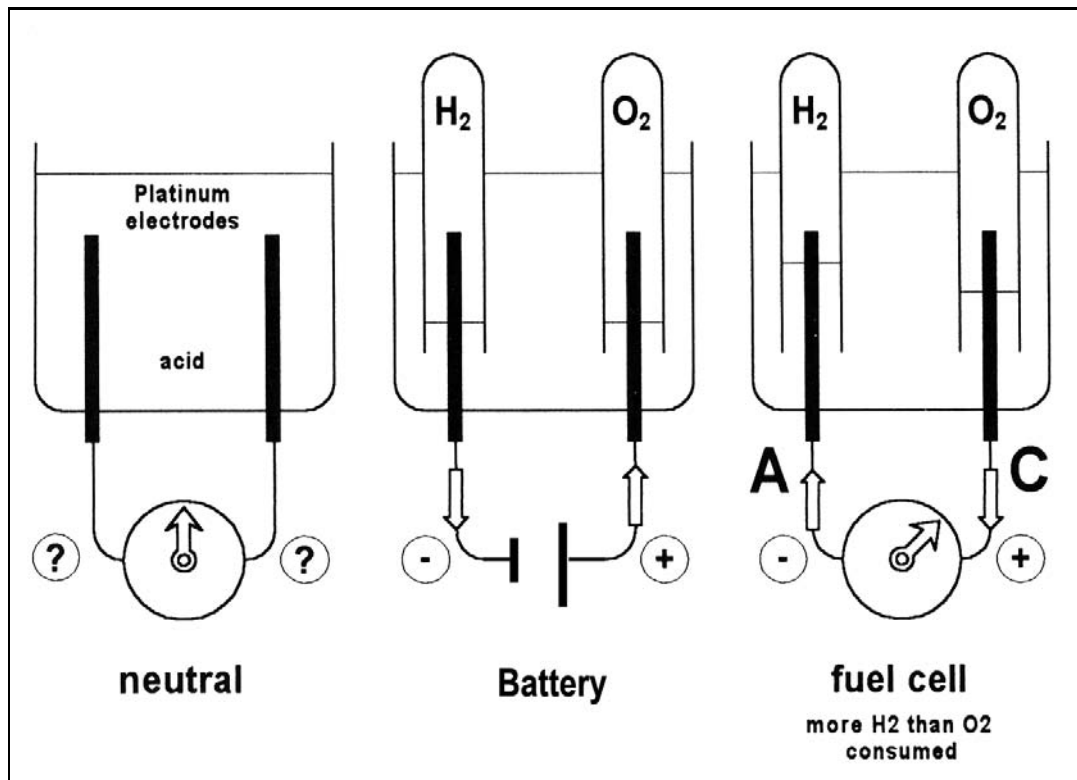


Figure 2.2: An illustration of Grove's Experiment of 1839.[1]

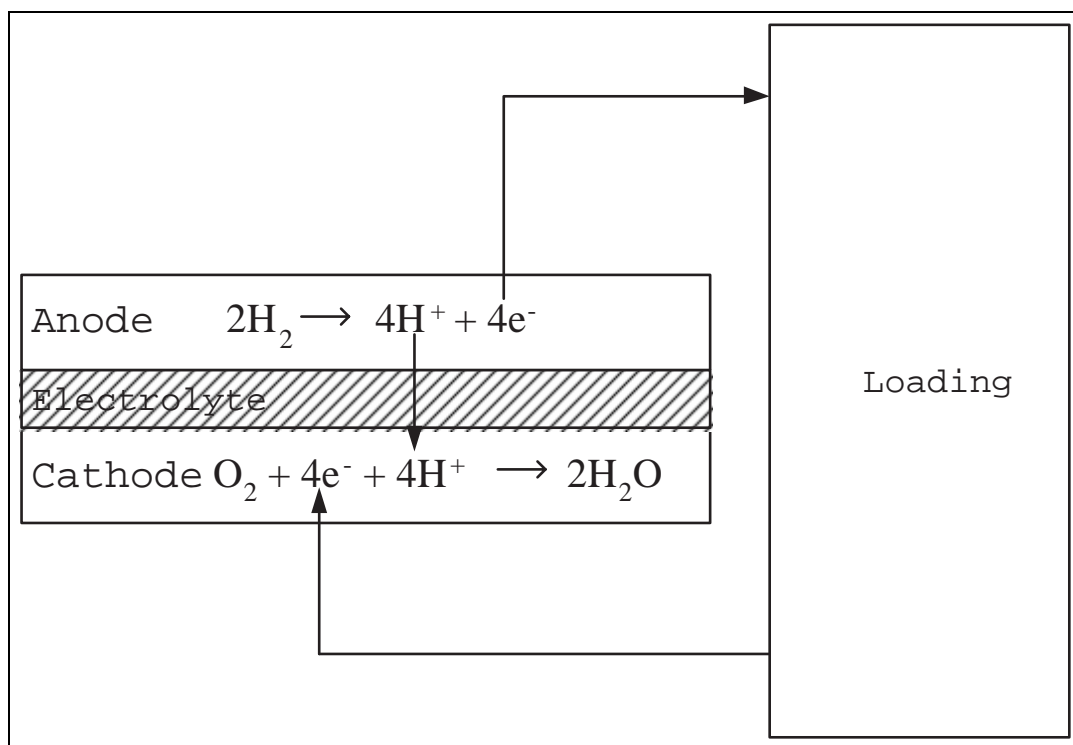
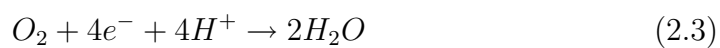


Figure 2.3: Basic construction of a hydrogen fuel cell



At the cathode, oxygen reacts with H^+ , and the electrons from the anode through external loading to form water.



By this simple reaction, a hydrogen fuel cell is able to provide energy as long as fuels are supplied.

2.3 Environmentally green energy source

Environmental concern is the biggest driving force of fuel cell development. Greenhouse gas, such as CO₂, NO and CO are produced in burning fossil fuel. In accordance with Figure 2.4, 50% of greenhouse gases are coming from fossil fuel combustion. Compared with turbine generator, solar cell or fuel cell can reduce the amount of greenhouse gases by 50%. Chlorofluorocarbons (CFCs) and other components contribute to the remaining 35% of greenhouse gases.

In a fuel cell, fuels are directly transformed into electricity without combustion. As a result, a fuel cell has virtually no gaseous or solid emission. In addition, it is also a high efficient energy source.

In some cases, one may argue that alternative energy sources, such as solar power, wind turbine etc., are even more environmentally green energy sources. However, their performance depends on the environment and physical location. On the contrary, a fuel cell can convert fuel energy into electricity in any place and at any time. Besides, its energy-conversion efficiency is higher than a steam generator or a combustion engine. Table 2.1 makes a comparison be-

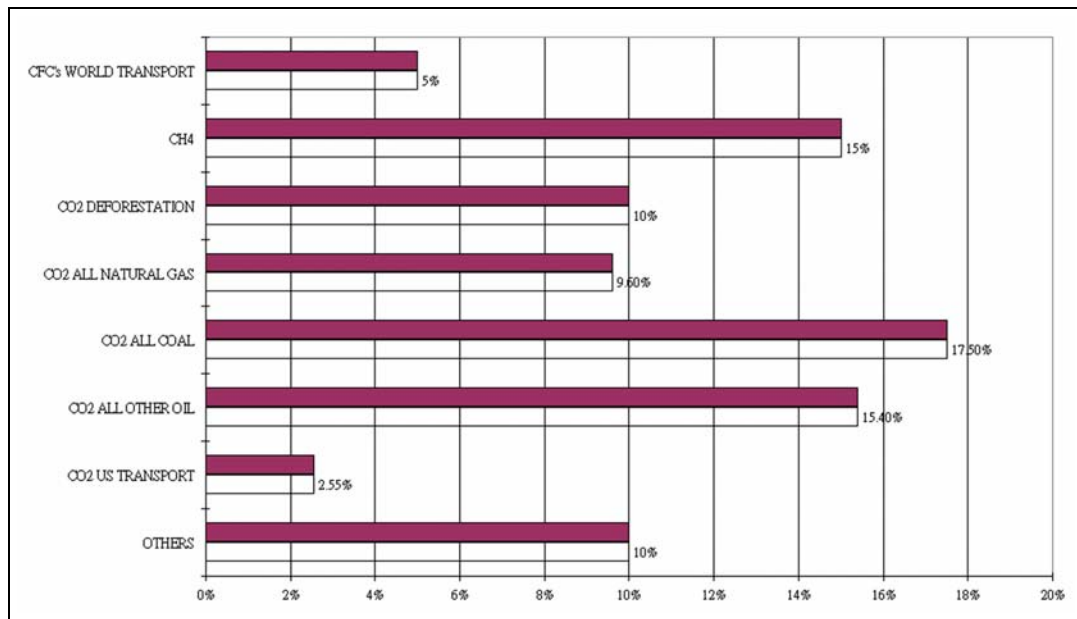


Figure 2.4: Partition of green house gases in ambient

tween several existing technologies, which indicates that fuel cell has a higher potential in the future. Besides, compared with others energy sources, fuel cell is a scalable, portable and high power density source, which make it different from others.

	Fuel Cell	Solar Cell	Wind Turbine
Size range(kilowatt)	$\leq 1 - 10000$	$\leq 1 - 1000$	$\leq 1 - 3000$
Energy conversion efficiency (percent)	35-50	-	-
Current installation cost (U.S.\$ per kilowatt)	\$2000-\$3500	\$5000-\$10 000	\$900-\$1000

Table 2.1: Comparison between existing technologies

2.4 Types of fuel cells

There are quite a number of types of fuel cell systems. Within each type, there are also a number of variations. Generally, in terms of the electrolytes used, they can be categorized into five categories. Their differences are summarized in Table 2.2. Different operating temperatures are required in different kinds of fuel cells. For high temperature fuel cells, the electrode kinetic activity is higher because higher reactivity rate is obtained under higher temperature. Therefore, high reactivity catalyst may not be required. Usually, it has a flatter loading characteristic and a better dynamic response because of the higher ion transfer rate inside the cell. In addition, It also has greater fuels impurity tolerance.

Conversely, low temperature fuel cells highly rely on the reactivity of catalysts. Precious materials, such as platinum, are used to promote the reaction on both the cathode and the anode side. Compared with high temperature fuel cell, it has relatively poor V-I characteristic. Moreover, poisoning of catalyst can happen on both anode and cathode.

High temperature fuel cell like Molten Carbonate Fuel Cell (MCFC) or Solid Oxide Fuel Cell (SOFC) do not need expensive catalysts. Moreover, it has the

	Proton Exchange Membrane Fuel cell (PEMFC)	Alkaline Fuel Cell (AFC)	Phosphoric Acid Fuel Cell (PAFC)	Molten Carbonate Fuel Cell (MCFC)	Solid Oxide Fuel Cell (SOFC)
Electrolyte	Ion Exchange Membrane	Concentrated Potassium Hydroxide	Immobilized Liquid Phosphoric Acid	Immobilized Liquid Molten Carbonate	Ceramic
Operating temperature	80°C	< 120°C	250°C	650°C	600°C - 1000°C
Charge Carrier	H ⁺	OH ⁻	H ⁺	CO ₃ ⁼	CO ₃ ⁼
External reformer for CH ₄	Yes	No	No	No	No
Prime cell components	Carbon-based	-	Graphite-based	Stainless steel	Ceramic
Catalyst	Platinum	Platinum	Platinum	Nickel	Perovskites
Product water management	Evaporative	-	Evaporative	Gaseous product	Gaseous product
Product heat management	Process gas and independent cooling medium	-	Process Gas Independent Cooling Medium	Internal reforming and process gas	Internal reforming and process gas

Table 2.2: Types of fuel cells

higher possibility to reform hydrogen from natural gas, methanol etc. inside the cell. Since the reaction inside the cell is exothermic and the hydrogen reforming is endothermic, the heat generated inside the cell can be reused to satisfy the heat requirement during the reforming state. Thus, the overall efficiency of such a system can be improved. In low temperature fuel cells, such as PEMFC, PAFC, internal reforming is not easy to achieve. Therefore, a separate external reformer may be required if pressurized hydrogen is not used.

Lower temperature operation of fuel cells has advantages and disadvantages. When supplied with pure hydrogen, it is able to startup under ambient condition quickly. Yet, it needs expensive platinum catalysts to promote the chemical reaction. Besides, the platinum catalysts are also sensitive to contamination from carbon dioxide (CO). Therefore, a filter for CO removal is desirable especially when a reformer is used. Moreover, the heat generated from a low temperature fuel cell is insufficient for recycling propose. Most important, the cell performance varies in accordance with temperature, fuel pressure and humidity. Thus, special attention should be paid to the overall system control to compensate these side effects.

Polymer Electrolyte Fuel Cell (PEFC) offers a relatively simpler structure. Here a solid polymer membrane is used to replaced alkaline electrolyte. This

kind of fuel cell is also known as “Proton Exchange Membrane Fuel Cell (PEMFC)” as protons are “exchanged” from anode to cathode through the solid polymer. The solid polymer membrane simplifies the complexity of sealing and the circulation of electrolyte. In addition, immediate startup is feasible in PEMFC. As a matter of fact, PEMFC is the most commonly used system at the moment, particularly in small scale and portable power systems.

Other than the PEFC, Direct Methanol Fuel Cell (DMFC) is also a popular candidate in portable applications such as mobile phones and laptop computers. Direct Methanol Fuel Cell (DMFC) draws attention of researchers due to the fact that methanol has a significant higher volumetric energy density compared with hydrogen fuel. Because methanol is directly injected into the fuel cell, it eliminates the need of a fuel processor. Therefore, DMFC has a significant lower volumetric scale compared with conventional fuel cell systems. Thus, DMFC has a very high good potential for portable devices.

However, in order to extract the hydrogen from methanol internally at room temperature, noble materials such as Pt and Ru alloy have to be used as a catalysts on the electrode. Beside, the CO gas generated can poison the catalysts and slow down its activity.

Methanol has the tendency of crossing the membrane from the anode side to

the cathode aside. This "cross-over" effect resulting in significant loss in potential and lowers the efficiency of the DMFC in the long run. The concentration of methanol can be controlled so as to minimized this effect. However, this increases the system complexity.

2.5 Structure of Proton Exchange Membrane Fuel Cell (PEMFC)

2.5.1 Membrane

Membrane is the most vital element in a fuel cell. It is an advancement that enables fuel cell to be operated at room temperature. The use of organic exchange membrane polymer was first reviewed by Willian T. Grubbs [3] in 1959. The polymer membrane was about 0.06mm thick and made of polystyrene with HSO_3 groups of sulfonic acid. It provides a conduction channel for hydrogen ions while acting as a gas barrier to prevent hydrogen gas flow directly to cathode.

Nowadays, one of the most commonly used membrane is Nafion from DuPont. As shown in Figure 2.5, Nafion 117 has a repeating polymer structure containing with carbon, fluorine, oxygen, sulfur and hydrogen. The hydrogen atom on

the SO_3 part of the molecule can be detached from the SO_3 site. The free H^+ proton can hop from one SO_3 site to another SO_3 site through the material, to emerge on the other side of the membrane. This is the reason why it is called proton exchange membrane. Here the solid sulfuric acid is used as an electrolyte.

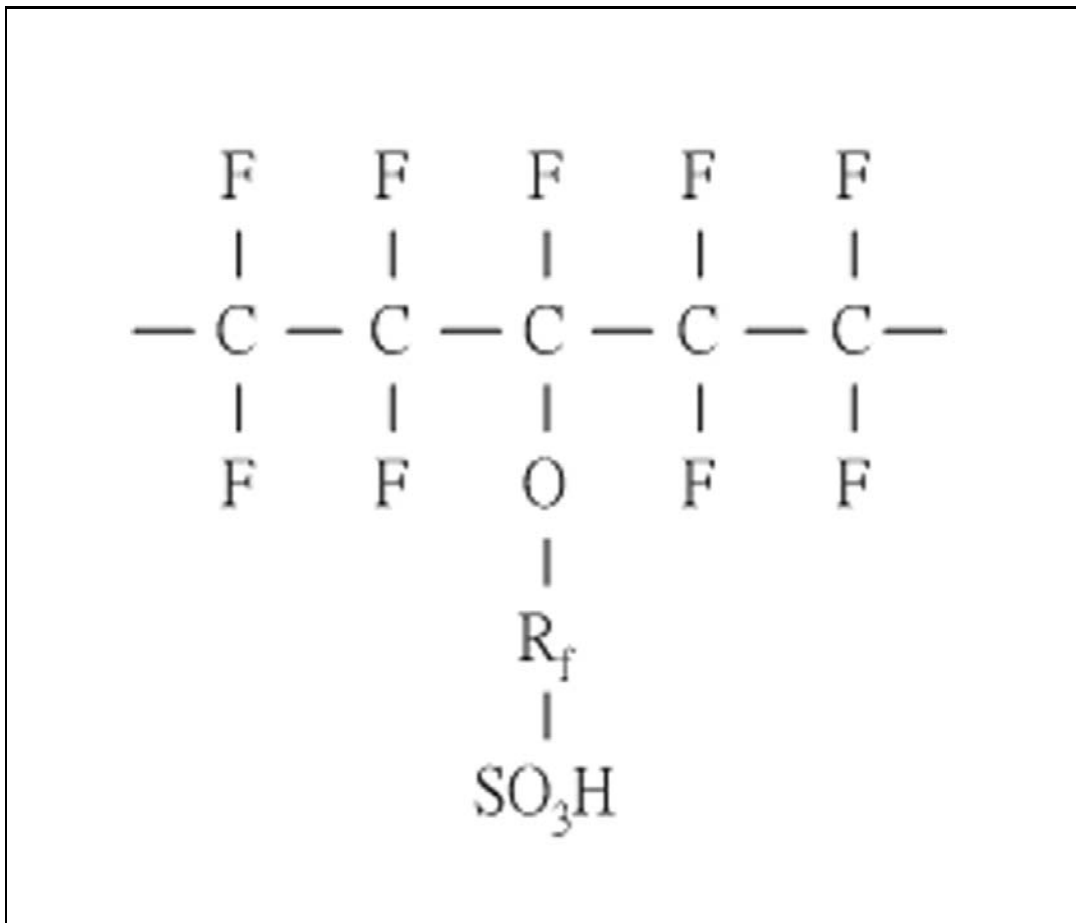


Figure 2.5: The structure of Nafion 117 from Dupont.

In order to maintain the mobility of proton, the membrane requires water.

The water content is an essential factor to determine the ionic conductivity of the membrane. Since water is produced as a byproduct in PEMFC operation, thus, this basic criteria can be satisfied. However, special attention have to be taken to ensure that an appropriate amount of water is remaining inside the PEMFC. More information will be given in Chapter 4.

2.5.1.1 Recent advancement

Recent research activities are focused on developing membranes with

- Higher proton conductivity.
- Thinner membrane thickness.
- Better mechanical stability.

The Dow Chemical Company and Ashai Chemical Company synthesized advanced perfluorosulfonic acid membranes with shorter side chains and higher SO_3H to CF_2 ratio [4]. It has a lower equivalent weight compare with Nafion 115. In addition, it has a significantly higher proton conductivity and shows a 50-100mV increase in cell potential at a loading of 1A/cm [4].

For ease of industrial assembly, the membrane is usually packed as a Membrane Electrode Assembly (as discuss in Chapter 2.5.3) with hot press. In this process, high mechanical stability is required. W.L.Gore and Associate man-

aged to improve the mechanical strength by supported membrane. Soubilized Nafion is incorporated in a fine-mesh Telfon support [5].

2.5.2 Electrodes and electrocatalyst

When a PEMFC is in operation, there is considerably voltage drop across electrodes. (The voltage drop across electrodes is regarded as overpotential in electrochemistry). For example, at current density of 1A/cm, the overpotential is 20mV at hydrogen electrode and 400mV at the oxygen electrode.

The exchange current density, i_0 , at the electrodes is a measure of the amount of electron-transfer activity in the equilibrium. In general, a larger current density of i_0 indicates a more rigorous process of simultaneous oxidation and reduction is taking place. The difference of the potential in the PEMFC from its reversible value (theoretical value of open circuit voltage) is due to the low exchange current density for oxygen. The current density of i_0 in the cathode can be much higher than that in anode. For example in a typical fuel cell, i_0 at the oxygen cathode can be 105 times higher than that at the hydrogen anode. In fact, oxygen reduction is more complex and difficult than oxidation of hydrogen in anode. Though, there is no conclusive argument that what intermediate steps are taken place in reduction of oxygen into water.

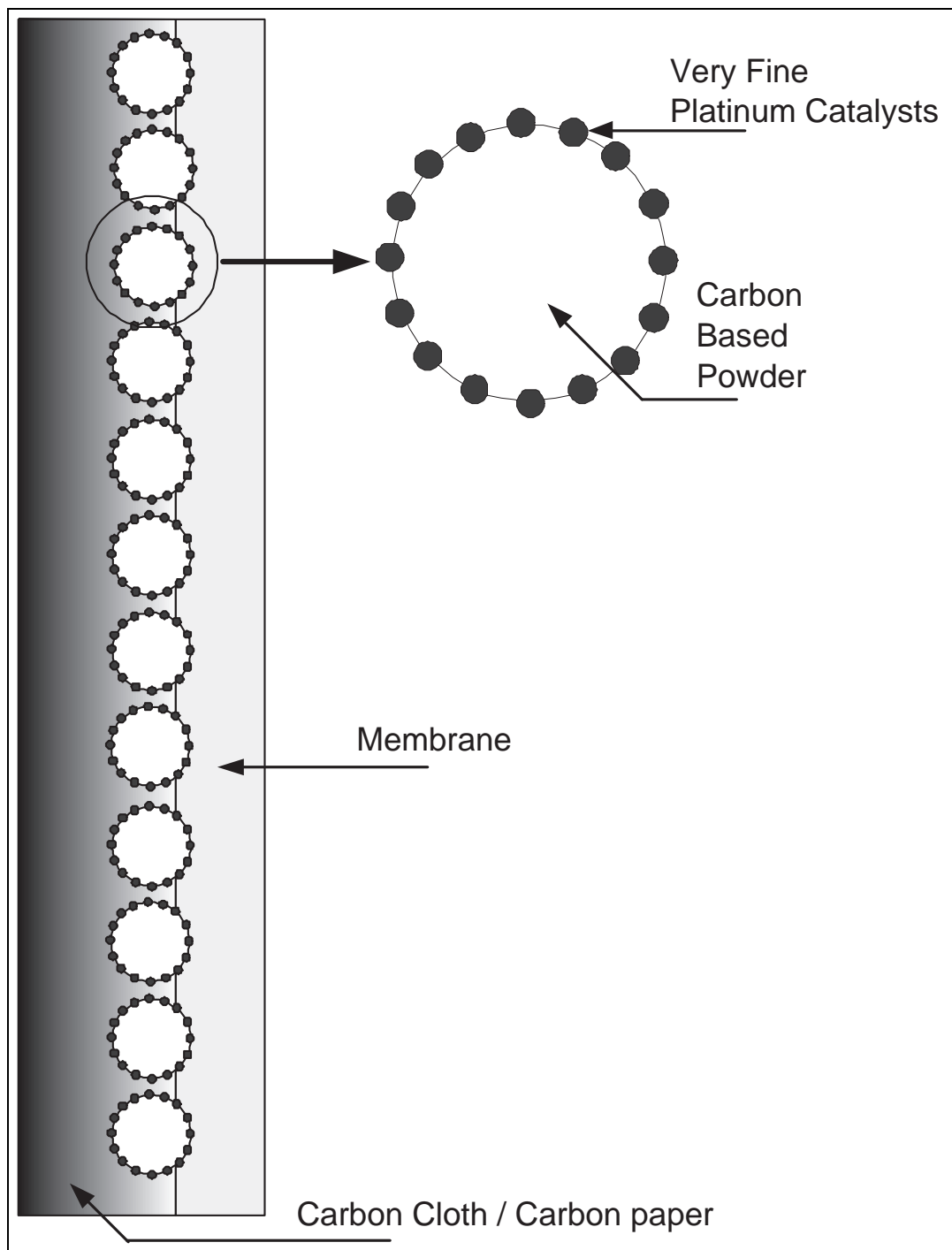


Figure 2.6: An illustration of a single PEMFC electrode structure and catalyst arrangement.

Thus for sake of lowering the i_o in the electrodes, Pt or Pt alloy is chosen. For low temperature fuel cell, such as PEMFC, the i_o is even higher. Despite of the high price of Pt and Pt alloy, they are still the best materials for PEMFC electrodes. As shown in Figure 2.6, porous or conductive material such as carbon paper or carbon cloth is used as a core material in the electrode. It provides electric conductivity and also provide as a channel for gas diffusion. Carbon based powder then is used as a supporting material for the very fine platinum catalyst.

To increase the power density, pressurized hydrogen cannot be considered. Instead, hydrogen may be reformed from natural gases, methanol or gasoline. Very often, a small quantity of carbon monoxide (CO) impurity is mixed in the hydrogen gas and fed into the anode. However, CO is preferentially absorbed by catalysts - Pt. In normal situation, Pt is only assumed to be used in dissociation of hydrogen into proton. Thus, this effect is lowering the capability of dissociative of hydrogen into proton. Therefore, special attention have to prevent this.

2.5.3 Membrane Electrode Assembly (MEA)

In commercial product, conventional way of connection electrode-membrane-electrode is rarely seen. Membrane Electrode Assembly (MEA), as shown in Figure 2.7, is now widely used by many PEMFC manufacturer including Ballard Power System of Canada and H-Power of United States as a reliable components. The fabrication of MEA can be summarized as below[6]:

1. The prepared membrane is cleaned by boiling water with 3% of hydrogen peroxide for one hour.
2. The cleaned membrane is immersed in the sulphuric acid for one hour.
3. The membrane is then immersed in the de-ionised water for one hour.
4. Electrode with catalyst is applied (sandwiched) on both side of the membrane.
5. The MEA is hot pressed at 140 °C

MEA can be prepared by high-volume manufacturing process which simplifies the assembly work. The life time of MEA can be as long as many thousands of hours with purified hydrogen as fuel. It can achieve a current density of 0.6A/cm² at 0.7V.

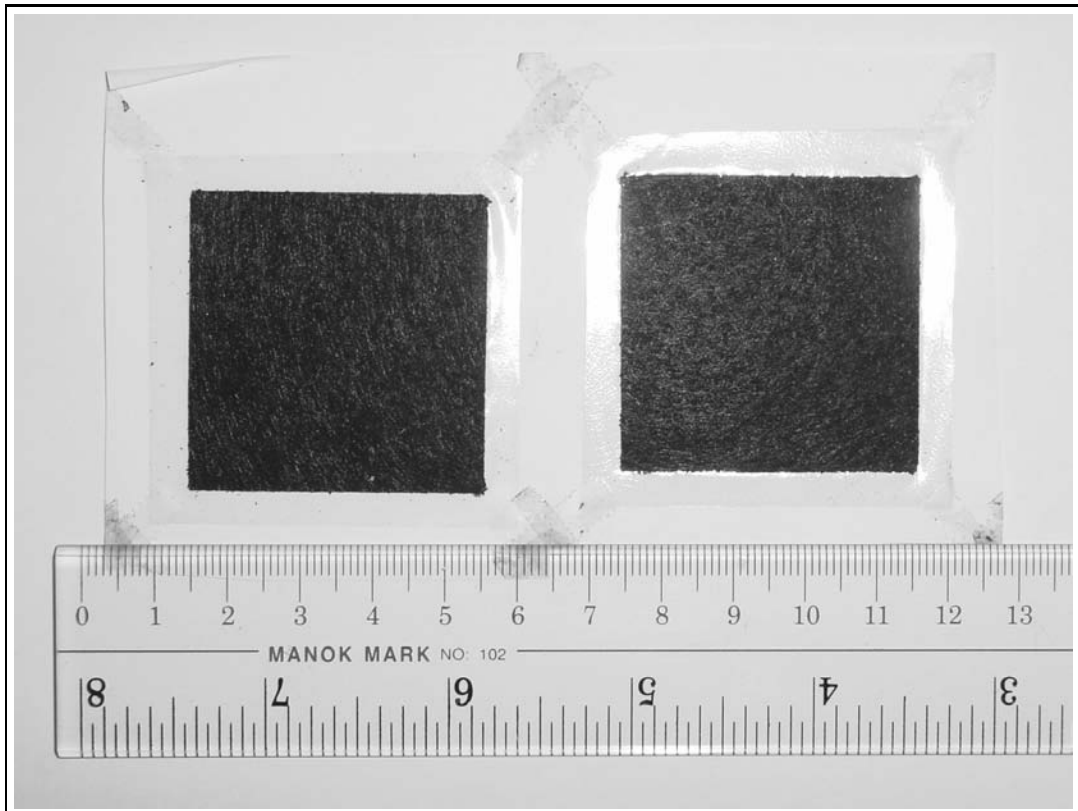


Figure 2.7: A commercialized Membrane Electrode Assembly (MEA).

2.5.3.1 Recent advancement

Lower cost and higher tolerance to CO are the key research objectives in MEA development.

Platinum is a precious material. In fact, the use of platinum is one of the obstacles that limit the wide use of fuel cells. To reduce the amount of platinum required on the electrode, supported platinum on high surface area is used, as illustrate in Figure 2.6. It can reduce the amount of platinum from $4\text{mg}/\text{cm}^2$ to $0.4\text{mg}/\text{cm}^2$ [7]. Another technique that has been developed to reduce the platinum loading to as low as $0.1\text{mg}/\text{cm}^2$ was reported in reference [8]. It provides $3\text{A}/\text{cm}^2$ at a voltage higher than 0.4V on pressurized O_2 , and $1\text{A}/\text{cm}^2$ at 0.65V .

Additional materials, Ru, Rh and Ir together with Pt were used in the 1960s by General Electric to improve the CO tolerance. Recent results show that the use of Pt-Ru with $1\text{mg}/\text{cm}^2$ of $\text{Pt}_{0.5}\text{Ru}_{0.5}$ can achieve an output of 0.4V of current density of $1\text{A}/\text{cm}^2$ with 250ppm of CO present in the hydrogen fuel [9].

2.5.4 Bi-polar plate

The primary function of a bi-polar plate is to separate individual cells from a stack. In addition, it also supplies fuel to the MEA through the flow channel while removing excessive water. Since the terminal voltage of PEMC is low, usually fuel cells are connected in series to establish a more useful voltage. Therefore, bi-polar plate also serves as a electrical conductor connecting individual PEMFC serially in the stack.

For this purpose, a bi-polar plate should have strong impermeability to hydrogen, oxygen and high resistance to chemical corrosion. Usually, it is made of carbon or metal like stainless steel or titanium. In addition, the surface of the bi-polar plate is machined with flow-field geometry to ensure even diffusion of fuel on the surface of the catalyst. The resistance of bi-polar plate should be as low as possible.

Figure 2.8 and Figure 2.9 show a practical bi-polar plate made of carbon composite. On the anode side, the flow pattern is rather simple. However, on the cathode side, the flow channel is specially designed to ensure a good balance of water content along the membrane. Indeed there are a number of flow pattern configurations available. In PEMFC, air flows from one end to other end along



Figure 2.8: An illustration of bi-polar plate on cathode side.

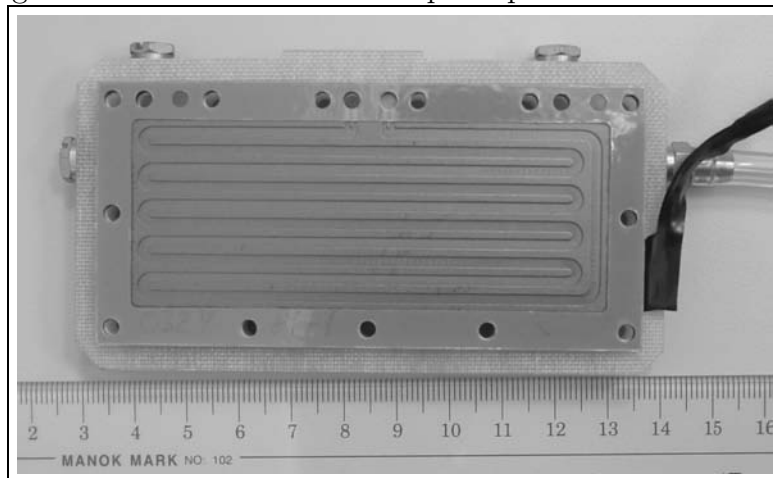


Figure 2.9: An illustration of bi-polar plate on anode side.

the fuel cell. Thus it is important to ensure that the water content and oxygen content are balanced along the whole journey. In some cases, the input air can be relatively dry while the output air at the ending can be extreme humid.

2.5.4.1 Recent advancement

Metals are good electric and thermal conductors with good mechanical strength and are easy to handle. However, it can hardly stand against chemical corrosion. Extensive research is now undertaken to overcome this weakness. Metal ions such as nickel ion contained in the stainless steel will poison the membrane by restricting proton transfer. Highly alloyed stainless steel contains high content of nickel and chromium and is therefore not suitable for fuel cell application. A common practice nowadays is to use stainless steel with covered passivation layer [10]. However, compared with conventional fuel cells, its voltage drops more severely along the surface resistance of the passivation oxide. Gold or titanium coating and titanium nitride layer are now proposed to be used as the passivation layer in stainless steel [11, 12].

2.6 Filling issue

Hydrogen is a flammable gas. 4% hydrogen content in air is enough to cause explosion. For public transportation, a flexible, safe and economical means of storage needs to be developed.

2.6.0.2 Pressurized hydrogen

Hydrogen is often stored in pressurized form to reduce the size of the container. Cylinder with different sizes and thicknesses can store different amount of hydrogen. The material used for the cylinder and the connection parts should be carefully selected. Hydrogen molecules are small and have high velocity. They are capable of diffusing into materials, which may eventually crack the material from the inside. Despite of this, it is the most common form of transportation at the moment.

An interesting calculation is given in Chapter 5 showing how long a hydrogen cylinder can sustain in real life operation.

	2 L steel, 200bar	147 L composite, 300bar
Mass of empty cylinder	3.0 kg	100 kg
Mass of hydrogen stored	0.0036 kg	3.1 kg
Storage efficiency (% mass of H ₂)	1.2 %	3.1%
Specific energy	0.47 kWh kg ⁻¹	1.2 kWh kg ⁻¹
Volume of tank	2.2L (0.0022m ³)	220L (0.22m ³)
Mass of H ₂ per liter	0.0016 kg L ⁻¹	0.0014 kg L ⁻¹

Table 2.3: Characteristic of pressurized system

2.6.0.3 Liquid hydrogen (LH₂)

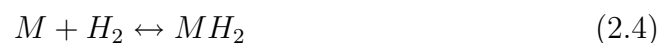
Liquid hydrogen is used in large power system such as NASA projectors power plant to carry large quantity of hydrogen. Several stages of energy intensive processes are required for the hydrogen-liquefaction. It involves about 40% of the specific enthalpy of hydrogen, resulting in low overall system efficiency. In addition, a heat exchange system is needed to gasify the liquid hydrogen for fuel cell operation. However, liquid hydrogen will remain in its place for a while even if the container cracks. Compared with a pressurized system, it could be safer.

	Cryogenic hydrogen container for car
Mass of empty cylinder	51.5 kg
Mass of hydrogen stored	8.5 kg
Storage efficiency (% mass of H ₂)	14.2 %
Specific energy	5.57 kWh kg ⁻¹
Volume of tank	0.2m ³
Mass of H ₂ per liter	0.0425 kg L ⁻¹

Table 2.4: Characteristic of liquified hydrogen system

2.6.0.4 Reversible Metal Hydride Storage

Metal hydride hydrogen storage is an inherently safe, low cost and low-pressure storage method that has been proposed. Here, hydrogen is stored by chemical process. Certain metals reacting with hydrogen can form metal hydride as shown in the equation below.



Cylinder containing metal hydride can store hydrogen at low pressure, approximately 2 bar. The reaction is reversible. Heat is produced when hydrogen is "recharging" and vice versa. Warm water or heat from ambient can speed up the hydrogen supply rate. Figure 2.10 shows an example of the metal hydride

container.



Figure 2.10: Metal hydride container.

2.6.0.5 Hydrogen reformer

Hydrocarbon fuels such as ammonia, methanol, ethanol etc. can be used as hydrogen carrier. Such a carrier has higher hydrogen carrying capability. However, the problem associated with it is the reforming process. In the reforming

	Metal Hydride Container
Mass of empty cylinder	0.26 kg
Mass of hydrogen stored	0.0017 kg
Storage efficiency (% mass of H ₂)	0.65 %
Specific energy	0.26 kWh kg ⁻¹
Volume of tank	0.06 L
Mass of H ₂ per liter	0.028 kg L ⁻¹

Table 2.5: Characteristic of metal hydride system

processing, CO and other grasses will be produced. Yet, the emission is lower that of combustion engine or power plant.

Chapter 3

Proton exchange membrane fuel cell system

3.1 Introduction

Proton exchange membrane fuel cell (PEMFC) can not operate in a standalone manner. It needs peripheral devices to support its operation. As illustrated in Figure 3.1, it need a fuel processor, a water management sub-system, an air management sub-system, a thermal management sub-system, and a power conditioner. In higher power applications, cell humidifier may also be used to enhance the system performance.

Compared with a conventional energy source, such as battery, the management

of PEMFC is considerably more complex. Thus, the design, optimization, and integration can also be very complex. Fuel efficiency, system stability, power density, fuel cell life and system flexibility can be ultimately altered by the system configuration and the operational strategies. Based on the block diagram shown in Figure 3.1, the operation of a typical PEMFC system is explained in the following sections.

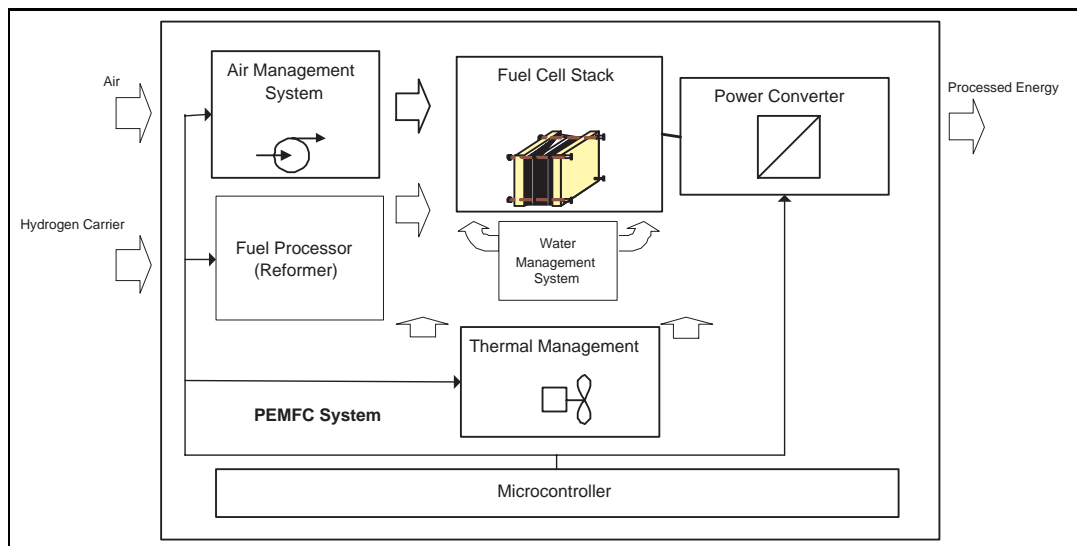


Figure 3.1: A Completed PEMFC System

3.2 Fuel processor (Reformer)

The fuel processor is used to reform hydrogen from an alternative fuel source. Hydrogen and oxygen are required by PEMFC. Oxygen can be extracted from the ambient air. However, hydrogen has to be supplied from external sources. The critical liquidation temperature of hydrogen is 33 K, which is well below the ambient temperature. It means that pure hydrogen can only be stored as gas in pressurized cylinders. Yet, in a modern composite tank, only 3% of the weight of the full cylinder is hydrogen [13]. Thus, many complementary methods have been invented to increase the fuel storage capacity.

The use of alternative hydrogen-carbon fuels such as gasoline, methanol and propane etc. for PEMFC is becoming popular. The advantages of using hydrogen-carbon fuel include high energy storage density and ease for transportation and handling. Unfortunately, the hydrogen content inside the fuel needs to be extracted by a fuel processor, which is also known as a reformer. Reforming process like steam reforming (SR) and partial oxidation (POX) are most commonly used nowadays. Notice that the carbon monoxide (CO) and carbon dioxide (CO₂) generated in the reforming process need to be removed to prevent contamination of the PEMFC catalyst.

However, the reforming process is usually regarded as an industrial scale process. It remains to be a challenge to scale down the whole process into a portable scale.

3.3 Air management sub-system

The air management sub-system is used to regulate the reactant pressure and flow rate to ensure proper operation of PEMFC. Other than fuel cells specially designed to consume pure oxygen, in general oxygen is taken from ambient. Pressurized air is continuously fed into one end of the cathode and exhausted from the other end of the cathode. This mechanism mainly performs two functions. First, it supplies the necessary oxygen for reaction. Second, the pressurized air removes excessive water generated during reaction.

The selection of fuel cell operation pressure, particularly that of the cathode, affects the performance of the fuel cell. Nernst equation, governing the deviation of cell voltage from theoretical value, reflects that a higher concentration of reactants can reduce the overpotential due to activation loss.

One thing that is usually ignored in system utilization is the energy consumption of the air compressor. The improvement due to the increase in reactants

pressure may not justify the energy used to pressurize the reactant gases.

3.4 Water management sub-system

The water management system is used to balance the water content inside the PEMFC. A PEMFC contains proton conductive material such as perfluorosulfonate ionmeric sandwiched between the anode and the cathode. The sulfonic acid group in the perfluorosulfonate ionmeric is essentially immobile and immersed in a fluoropolymer matrix. However, in a well hydrated membrane, the protons are weakly attracted to the sulfonic acid group and are able to move.

By this mechanism, even in room temperature, protons are allowed to “be exchanged” across the membrane from anode to cathode inside the PEMFC. Therefore, in order to maintain a sufficient reaction in the membrane, proper hydration in the membrane is required.

For self-humidified PEMFC, the water generated during operation is reused to humidify the membrane. This mechanism not only reduces the necessary water for the external-humidifier, but also prevents the risk of contamination

from external. However, the water management sub-system should prevent the cell from being too dry or flooded. Flow channels can be designed to reduce the unbalanced distribution of water content in the membrane [14]. Since the humidity cannot be directly controlled by external-humidifier, the water management sub-system can adjust the hydration of the membrane only indirectly through parameters such as fuel cell temperature, reactants flow rate or reactants pressure.

3.5 Thermal management sub-system

The thermal management sub-system is used for heat removal. Heat is released when the fuel cell is running.

In fact, the kinetic of the reactants increases for higher temperature. In principle, it reduces the overpotential due to mass transfer and ohmic losses. However, since the relative humidity is sensitive to temperature, the resultant effect could not be necessarily a plus.

The fuel cell temperature has to be kept at an optimal level. Otherwise, if the fuel cell does not have sufficient cooling, the warm air accumulated inside could “take away” all the water produced by the fuel cell. Eventually, the

membrane will become too dry and unable to operate.

A fan is commonly used for cooling in the PEMFC system. Depending on the the cooling-effectiveness (η_{them}) of the thermal management sub-system, it might consume approximately 1% to 4% of the electrical energy from the fuel cell.

Whether or not to activate the cooling system depends on designer's intention and availability of resources. In section 4.5, more specific details will be presented.

3.6 Power conditioner

Since the voltage output from the PEMFC is subjected to the variation in humidity, reactant pressure, current density etc., the terminal output voltage tends to be unstable. Usually, the energy from the PEMFC needs to be further processed before it can be used.

3.6.1 DC regulation

The operation voltage of each PEMFC cell is between 0.4 to 0.7 volts. Assuming a stack of 40 cells in series, it outputs a voltage of 16 to 28 volts, which is often too low for efficient operation. Besides, the voltage is unstable. A DC/DC converter is therefore commonly used to step-up and regulate the output voltage. Moreover, the DC/DC converter provides the necessary protection to avoid overloading. Half-bridge or full-bridge DC/DC converters are often used for such applications [15, 16, 17].

3.6.2 AC conversion

In many applications, such as uninterruptible power supplies (UPS), alternating current (AC) is required. In this situation, conversion from DC to AC is necessary. Similarly, a half-bridge or full-bridge topology can be adopted. Equipped with an LC output filter, the square wave output of the converter is reshaped into a near-sinusoidal waveform.

Compared with conventional battery, the internal resistance of a PEMFC is greater. In fact, the slow transient responses and start up delay place great challenges to the PEMFC system designers.

Chapter 4

Model of PEMFC system

Since the early 1960s, a number of fuel cell modeling techniques have been presented. These modeling studies predict the fuel cell half-cell potential (E) versus current density A/cm^2 behavior. In general, it can be classified in to two main categories, mechanistic model and empirical model. The mechanical model[18, 19, 20, 21, 22] focuses on the diffusion activities and activities of species in different stages.

When overpotential such as activation overpotential, mass transport, ohmic loss are all considered, especially when air is used in cathode as reactant, no analytic solution can be found in the mechanical model. From that point of view, the interpolation of half-cell-potential versus current density characteristics using empirical model [23, 24, 25, 26] is highly desirable.

Next section will focus on the modeling of a self-humidified PEMFC. It is assumed here that pressurized hydrogen is used. Therefore the fuel processor will not be considered. Crucial mathematical equations will be given in this section. In order to simplify the model, a number of assumptions are made and explained in each subsection.

4.1 Loading characteristic

The empirical model given by Amphlette et al. [27, 31], is used in this thesis as a fundamental core of the model to present the fuel cell characteristic in steady state. The terminal voltage for a single PEMFC is

$$V = E + \eta_{act} + \eta_{ohmic} + \eta_{proton} \quad (4.1)$$

where E is the theoretical reversible cell voltage, for electronics engineer, it is usually regarded as the open circuit voltage (OCV) and η_{act} is the activation overpotential. Activation overpotential was first reported by Tafel in 1905. It is an electrochemical effect related to the activity in electrodes. As mentioned in Chapter 2, the exchange current density, i_o , reflects the reactivity of the electrode. i_o can be determined by experimental method, the details of which

are outside the scope of this thesis. To make it simple, i_o is related to the effectiveness of the absorption of the reactants, the speed of the transfer of electrons across the double layer and the catalyst used in the electrode etc.

Referring to the Eq. (4.1), η_{act} is given by

$$\eta_{act} = \xi_1 + \xi_2 T_s + \xi_3 \ln(C_{O_2}^*) + \xi_4 \ln(I) \quad (4.2)$$

where ξ_1 , ξ_2 and ξ_3 are constants determined from the regression model presented by Amplette et al. [27, 31], T_s is the critical temperature, $C_{O_2}^*$ is the effective concentration of oxygen in mole/cm³ and I is the current density in A/cm².

The ohmic overpotential (η_{ohmic}) is related to the purely internal electrical resistance by the equation

$$\eta_{ohmic} = -(IR_{internal}) \quad (4.3)$$

To be precise, the $R_{internal}$ can be expressed as follows:

$$R_{internal} = 0.0165 - 3.5 \cdot 10^{-5}T + 8.0 \cdot 10^{-5}I \quad (4.4)$$

The constants in Eq. (4.4) can be varied in accordance with material used. It can be calibrated by regression technique with experimental data.

The additional term η_{proton} is the overpotential due to proton conductivity in the membrane, which will be explained later in section 4.4.

4.2 Reactants flow rate

Hydrogen and oxygen are used in fuel cell system. Usually, hydrogen is used in the anode with one end closed. As impurities may contaminate in the hydrogen, in practice, an electrically controlled valve will be used to conduct a periodic purge in anode gas.

The partition of oxygen in air is approximately 30%. Therefore, in real application, air, instead of pure oxygen, will be used in cathode. Air is circulated around the cathode to provide the necessary oxygen. As the same time, it also removes excessive water from the cathode to prevent flooding. In some cases, in order to shorten the start up time of a PEMFC system, an external humidifier is used to humidify the cathode.

Theoretically, the rate of usage of reactant is proportional to the current. As one oxygen molecule can provide four electrons and one hydrogen molecule can provide two electrons. The minimum flow rates of oxygen and hydrogen are respectively

$$\dot{m}_{\text{O}_2,\text{react}} = M_{\text{O}_2} \frac{I}{4F} \quad , \quad \dot{m}_{\text{H}_2,\text{react}} = M_{\text{H}_2} \frac{I}{2F} \quad (4.5)$$

where F is the Faraday constant, M_{O_2} and M_{H_2} are the molar mass of oxygen and hydrogen respectively.

As mentioned before, oxygen is extracted from air, the actual flow rate of air (\dot{m}_{air}) is

$$\dot{m}_{\text{air}} = M_{\text{air}} \nu_{\text{O}_2} \frac{I}{4F} \frac{1}{\gamma} \quad (4.6)$$

where γ is the molar proportion of oxygen in air and ν_{O_2} is the stoichiometric rate of oxygen in cathode. In fact, insufficient oxygen will introduce serve loss in the mass transfer, especially in high current density region. The details of this mechanism has been mentioned in the section 3.3. It is common to supply more oxygen than needed. Note that in Eq. (4.6), ν_{O_2} represents how many times more oxygen is actually supplied.

From Eq. (4.6), the power consumption of the air compressor P_{comp} can be calculated [28].

$$P_{\text{comp}} = c_p \frac{T_1}{\eta_C} \left(\left(\frac{P_2}{P_1} \right)^{\frac{\gamma-1}{\gamma}} - 1 \right) \dot{m}_{\text{air}} \quad (4.7)$$

where P_1 and P_2 are the inlet and outlet pressures of the compressor, T_1 is the inlet temperature of the gas in K, η_C is the isentropic efficiency and \dot{m}_{air} is the flow rate of the gas in kg/ s.

4.3 Water management sub-system

This section will present a simplified equation showing the relationship between proton conductivity (η_{proton}) and water activity (a) in the PEMFC. We will go through two stages. First, the change in relative humidity due to water generation will be found [28]. Second, the relationship between water activity and proton conductivity will be determined [29, 32].

4.3.1 Water activity

This section will try to derive a parameter a . a can be regarded as the relative humidity, which is very sensitive to temperature. This parameter is widely used in fuel cell models when determining the drying capability of air inside the fuel cell. Temperature is one of the important parameters that determines a . For example, if we conserve a jar of air with 70% relative humidity, sealed at 20°C , and then heat it up to 60°C , the relative humidity will become 8%, which is extremely dry. Therefore, when the PEMFC is heated up from 20°C to 60°C , and if water is not generated internally, the drying effect can be enormously high.

Assume that the water generated in the cathode side is in vapor form. There-

fore, the rate of water vapor production (\dot{m}_{vapor}) is

$$\dot{m}_{\text{vapor}} = M_{\text{vapor}} \frac{I}{2F} \quad (4.8)$$

where M_{vapor} is the molar mass of vapor in gram/mole.

Subtracting the air flow in (\dot{m}_{air}) by the oxygen used (\dot{m}_{O_2}), the rate of exiting air ($\dot{m}_{\text{air,exit}}$) can be deduced.

$$\begin{aligned} \dot{m}_{\text{air,exit}} &= M_{\text{air}} \nu_{\text{O}_2} \frac{I}{4F} \frac{1}{\gamma} - M_{\text{O}_2} \frac{I}{4F} \\ &= \frac{I}{4F} (M_{\text{air}} \nu_{\text{O}_2} \frac{1}{\gamma} - M_{\text{O}_2}) \end{aligned} \quad (4.9)$$

If the water content of inlet air is ignored, by combining Eq. (4.5) and Eq. (4.9), the humidity ratio of the air (ω_{exit}) leaving the cell can be found.

$$\begin{aligned} \omega_{\text{exit}} &= \frac{\dot{m}_{\text{vapor}}}{\dot{m}_{\text{air,exit}}} \\ &= \frac{2M_{\text{O}_2}}{M_{\text{air}} \nu_{\text{O}_2} \frac{1}{\gamma} - M_{\text{O}_2}} \end{aligned} \quad (4.10)$$

It is assumed that all the water generated is evaporated and that the water vapor and air behave as perfect gases. Therefore, on the other hands, the humidity ratio of the air (ω_{exit}) can also be deduced.

$$\omega_{\text{exit}} = \frac{M_{\text{H}_2\text{O}} P_{\text{vapor}}}{M_{\text{air}} P_{\text{air}}} \quad (4.11)$$

where P_{vapor} and P_{air} are the water vapor pressure and inlet air pressure in atm.

The total air pressure is the sum of the dry air and water vapor pressures. Thus

$$\begin{aligned} P_{\text{total}} &= P_{\text{air}} + P_{\text{vapor}} \\ \Rightarrow P_{\text{air}} &= P_{\text{total}} - P_{\text{vapor}} \end{aligned} \quad (4.12)$$

Combining Eq. (4.11) and Eq. (4.12), the humidity ratio of the exit air can be expressed as

$$\omega_{\text{exit}} = \frac{M_{\text{H}_2\text{O}}}{M_{\text{air}}} \frac{P_{\text{vapor}}}{P_{\text{total}} - P_{\text{vapor}}} \quad (4.13)$$

Equating Eq. (4.10) and Eq. (4.13), the pressure of the water vapor can be expressed as

$$P_{\text{vapor}} = \frac{2\gamma M_{\text{air}} P_{\text{total}}}{2\gamma M_{\text{air}} + M_{\text{air}} \nu_{\text{O}_2} - M_{\text{O}_2} \gamma} \quad (4.14)$$

Finally, if we further assume that the partial pressure of water vapor on the surface of the electrode is equal to the water vapor pressure on the surface of the membrane, it can be deduced that the water vapor activity, a , is

$$a = \frac{P_{\text{vapor}}}{P_{\text{sat}}} \quad (4.15)$$

where P_{sat} is the partial pressure of the water at equilibrium.

The saturated vapor pressure increases with temperature. If the saturated vapor pressure is reached, it can neither “take away” nor “absorb” any water.

P_{sat} can be equated as a function of temperature in °C [30].

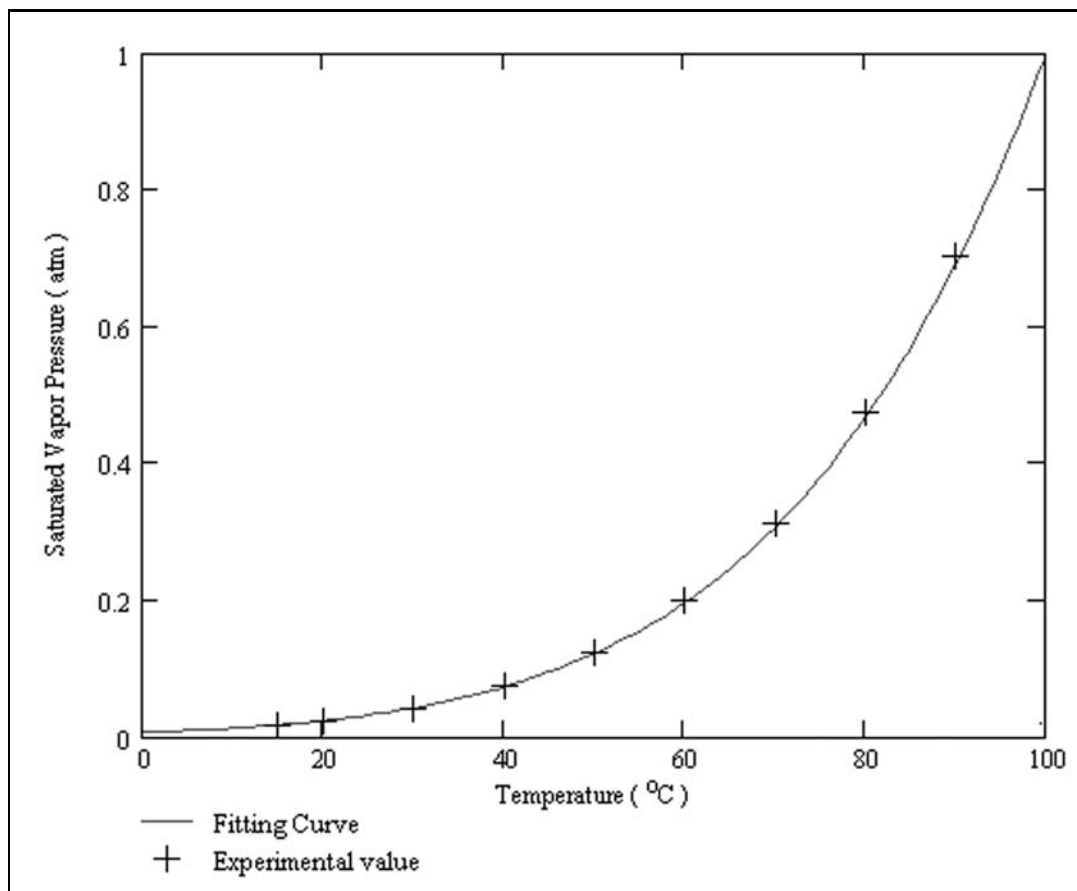


Figure 4.1: Saturated vapor pressure

$$\log P_{\text{sat}} = -2.1794 + 0.002953 \times T - 9.1837 \times 10^{-5} \times T^2 + 1.4454 \times 10^{-7} \times T^3 \quad (4.16)$$

4.4 Proton conductivity in membrane

Higher value of membrane hydration, λ , reflects greater content of water in the membrane. An empirical correlation based on the water content was measured by Zawodzinski for Nafion 117 at 30°C [29, 32]. An experimental relationship between membrane hydration and water vapor activity, a , is given below.

$$\lambda = 0.043 + 17.81a - 39.85a^2 + 36.0a^3 \quad \text{for } 0 < a \leq 1 \quad (4.17)$$

Assuming that hydration varies linearly from 14 to 16.8, the value of λ for $1 < a \leq 3$ can be found as [32]

$$\lambda = 14 + 1.4(a - 1) \quad \text{for } 1 < a \leq 3 \quad (4.18)$$

As given by Mann et al. [31], the conductivity of the membrane (σ) in $\Omega \cdot \text{cm}$ as a function of λ and temperature in K is

$$\sigma = \frac{[\lambda - 0.634 - 3 \times I] \exp\left(4.18 \left[\frac{T-303}{T}\right]\right)}{181.6 \left[1 + 0.03 \times I + 0.062 \left(\frac{T}{303}\right)^2 \times I^{2.5}\right]} \quad \text{for } \lambda > 1. \quad (4.19)$$

Finally the overpotential due to proton conductivity can be found.

$$\eta_{\text{proton}} = \frac{\sigma \times I}{t_m} \quad (4.20)$$

where t_m is the thickness of the membrane in cm.

4.5 Thermal management sub-system

Assume that no back pressure is created when the fan is switched on, and that the removal of heat is dominated by the convection of air. If the energy loss due to the ohmic resistance is transformed into heat, then we can equate the heat loss of the fuel cell as

$$P_{\text{heatlost}} = IR_{\text{internal}} \quad (4.21)$$

If a single DC-axial fan is used for heat removal, the electrical energy required is related to the cooling system effectiveness, η_{them} , by the following relationship

$$P_{\text{thermal}} = \frac{P_{\text{heatlost}}}{\eta_{\text{them}}} \quad (4.22)$$

In this section, we have studied the equations for each management sub-system.

For an end-user, the common concerns are output voltage, current, fuel efficiency and fuel cell lifetime. Based on input parameters such as reactant pressure, flow rate and temperature, these concerns will be considered in the following sections.

The model presented in this sectioned was simulated by MathCad 2000. The details of the documentation are shown in the Appendix. The result presented in the next section were calculated based on the parameter given in the Table 4.1.

Parameters	Value	Unit
ξ_1	-0.944	-
ξ_2	0.00354	-
ξ_3	$7.8 \cdot 10^{-5}$	-
ξ_4	-0.00019	-
E	1.2	Voltage (V)
F	96485	Coulombs (C)
M_{O_2}	$32 \cdot 10^{-3}$	grams/mole
M_{H_2}	$2.02 \cdot 10^{-3}$	grams/mole
M_{air}	$28.97 \cdot 10^{-3}$	grams/mole
t_m	0.0017	cm
ν_{O_2}	2	-
γ	1.4	-
c_p	1004	-

Table 4.1: Parameter for simulation

4.6 Elaboration on the PEMFC Model

Figure 4.2 illustrates the effect of temperature on fuel cell performance. In general, a higher operational temperature results a higher voltage in the low current density region. However, as the current density increases, this advantage may disappear. For temperatures higher than 90°C, only marginal voltage difference is observed in the low current density region. Figure 4.2 illustrates the resultant overpotentials against current density. It is observed that while the activation overpotential decreases, the saturated vapor pressure due to temperature rises. Thus, higher operation temperature seems to be benefiting PEMFC. However, as the current density increases, this benefit may vanish as the saturated vapor pressure starts to dehydrate the membrane causing a detrimental impact.

As illustrated in Figure 4.3, since ohmic losses due to membrane always exists, temperature rise in an operating PEMFC is inevitable. In the high current density region, nearly 50% of fuel energy is wasted as heat. To recover the heat loss, it is necessary to minimize the loss due to membrane resistance, or to reuse the heat generated.

Pressurized gas can help reducing the activation overpotential, especially in

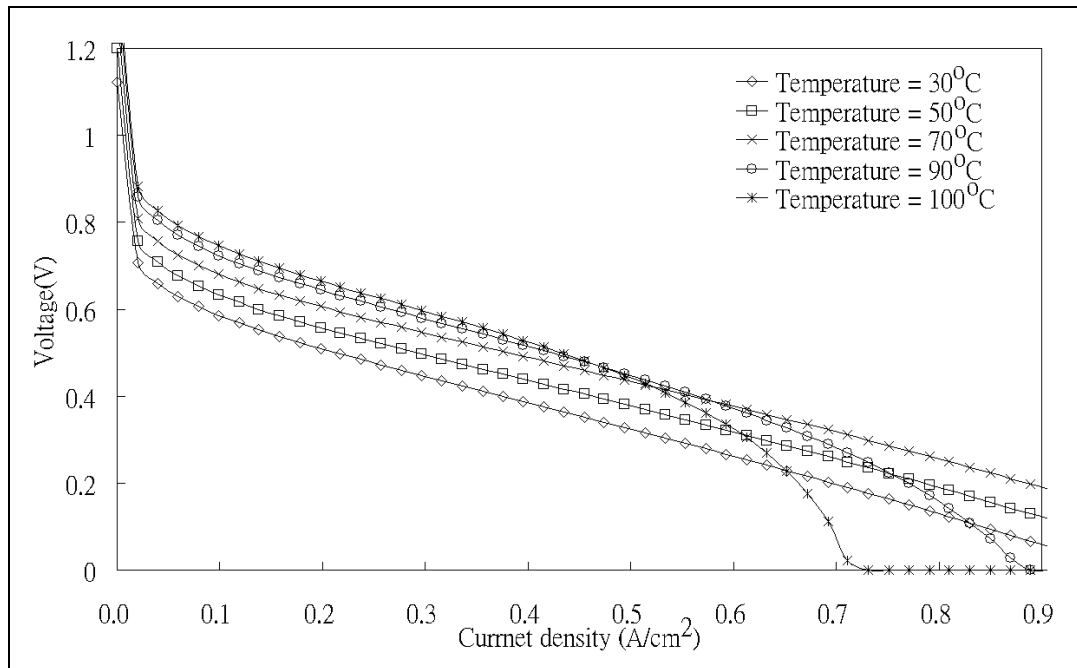


Figure 4.2: Effect of temperature: Cell potential against current density plot with inlet pressure at 2 atm and stoichiometric rate set at 2.

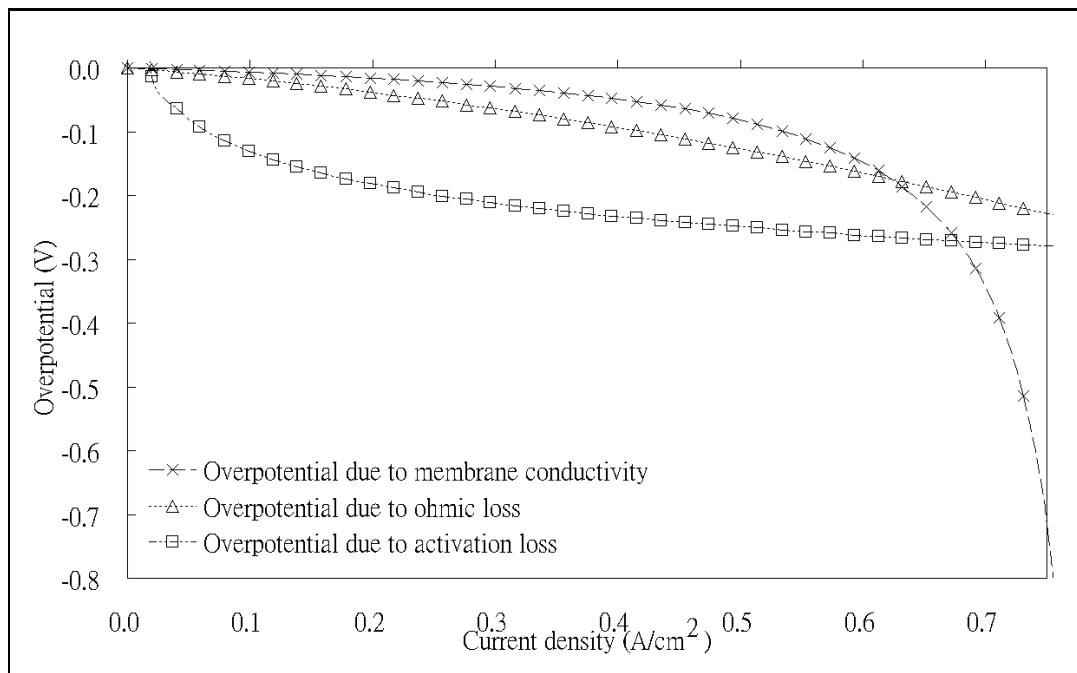


Figure 4.3: Overpotentials due to temperature at 100°C.

the cathode. Figure 4.4 shows the PEMFC performance for different air pressures. At 1 atm level, a significantly higher slope is observed compared with other operational pressures. Noticeably, the difference is even more in the high current density region. It is due to the fact that the mass-transport-limitation is reached earlier than expected. Indeed, experimental results [33] conclude that the drop of pressure in the cathode, especially in the technologically significant case of 1 atm, has significant impact in the medium to high current density range. In general, increased pressure in cathode increases the power density.

However, high operational pressure may not be practically feasible.

As seen in Figure 4.5, if the operational pressure is set at 4 atm, nearly half of the electrical energy output from the PEMFC is used in pressurizing the air. Therefore, in normal operation, the cathode reactant pressure should be set between 1 to 2 atm, so as to achieve a balance between the gain in power and the energy loss due to pressurization.

Finally, Figure 4.6 demonstrates how the flow of air can affect the PEMFC performance. As the stoichiometric rate increases, the dehydration effect due to air increases. In the high current density region, severe loss in voltage can be seen. Usually, the flow of the air is controlled such that the resultant flow

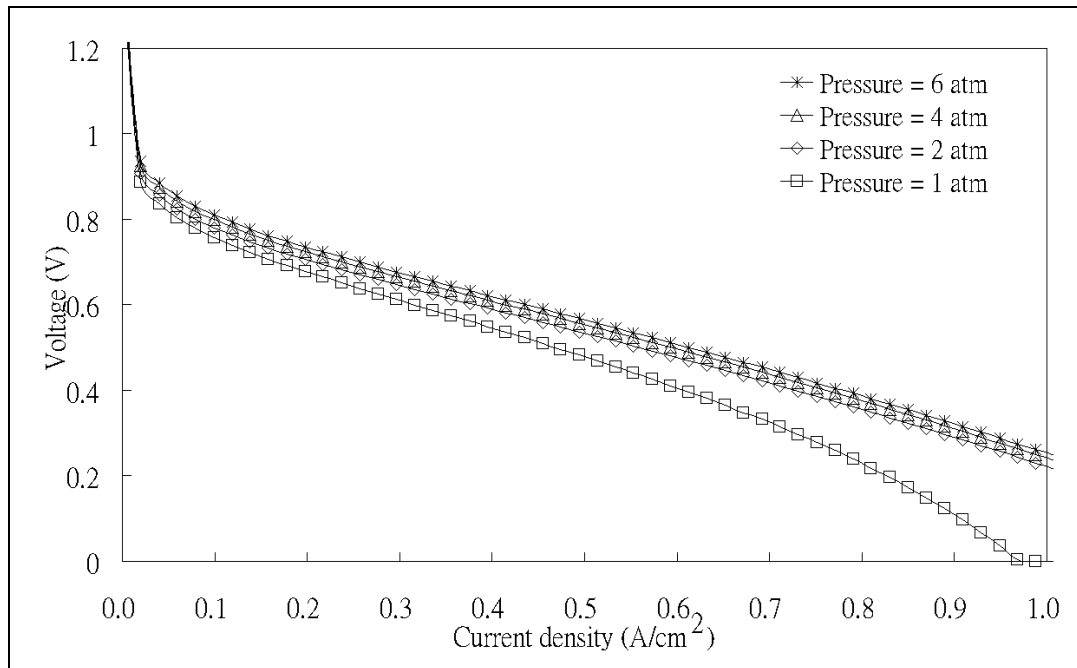


Figure 4.4: Effect of Cell potential against current density plot with PEMFC temperature kept at 70°C and stoichiometric rate set at 2.

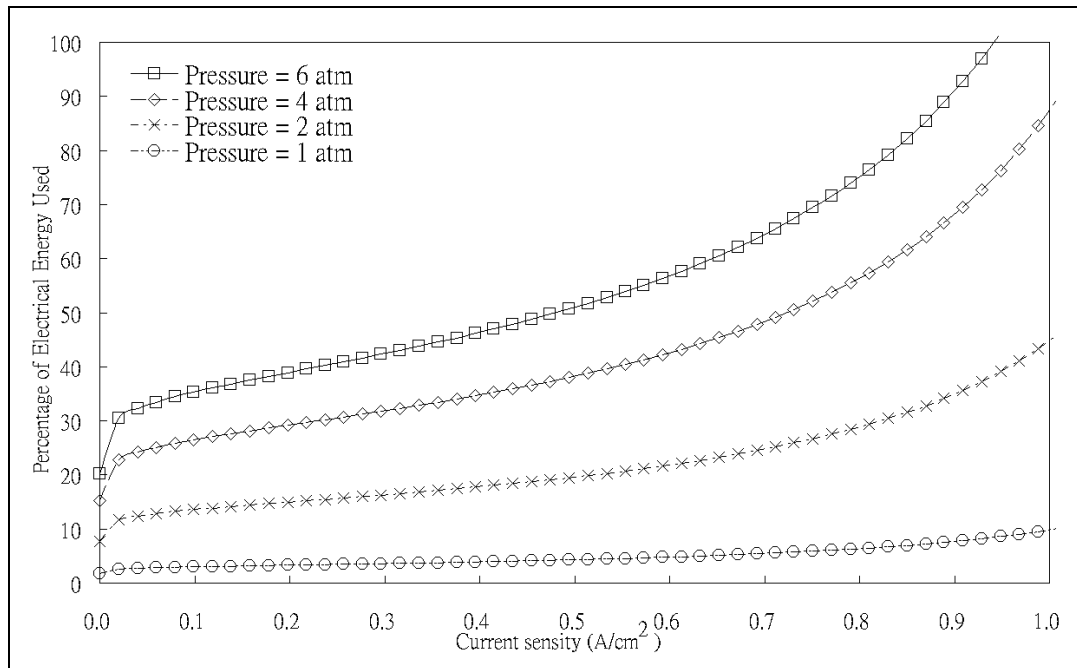


Figure 4.5: Percentage of energy used by the compressor with respect to the PEMFC electrical output.

of oxygen is approximately twice as much as needed. The objective here is to provide sufficient oxygen while reducing the dehydration effect to minimal.

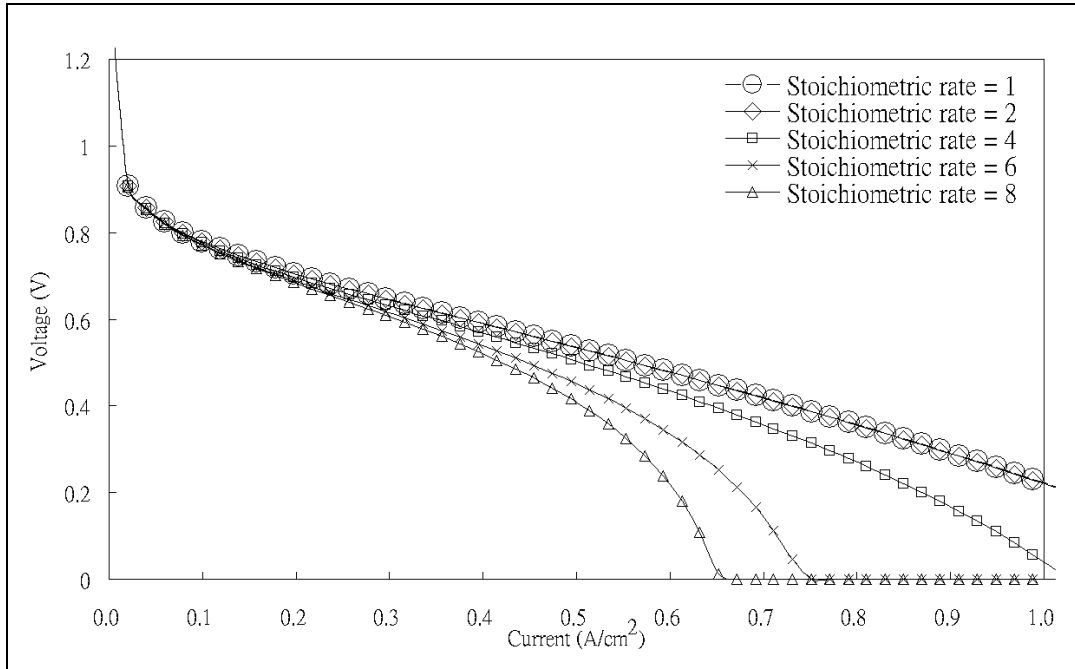


Figure 4.6: Effect of stoichiometric rate: Cell potential against current density plot with inlet pressure at 2 atm and PEMFC temperature kept at 70°C.

A complete PEMFC system contains several management units. Depending on the user's intention and application, different configuration and optimization strategies can be implemented. To fulfill certain operational requirements, it is common to accept trade-offs. In this section, we have studied the influence of controllable parameters. In the next section, certain operation modes are

outlined for references as listed in Table 4.2.

Operation modes	Features	Trade-offs	Strategies
Initialization mode	Initialize a PEMFC that has not been used for a long time		Load the cell with medium to high current and keep the stoichiometric rate to minimal
Standby mode	Shorten the time taken for a PEMFC to reach full-load operation	Continuous operation is required	Apply periodic loading
Boost mode	Provide extra power to meet occasional peak requirements	Severe heat lost and low efficiency	Pressurize air supply

Table 4.2: Summary of suggested operation mode.

4.6.1 Initialization mode

For a PEMFC that has not been used for a long time, the hydration level of the membrane can be very low. This reduces the proton conductivity of the PEMFC and reduces the output power of the PEMFC. The membrane hydration, λ , of a fresh start up fuel cell can be so low that it will prevent nearly half of the reaction from taking place between electrodes, compared with usual operation. Therefore, it is important to increase the value of λ at the start up period. In other words, it is necessary to increase the proton conductivity by increasing the internal humidity of the PEMFC.

For self humidified fuel cell, the water generated during operation is used to humidify the membrane. In the initialization mode, the fuel cell should preferably have a large loading current. On the other hand, the stoichiometric rate in cathode should be maintained relatively low. This act can ensure that the water vapor generated during reaction can remain inside the fuel cell to humidify the membrane. Figure 4.7 gives an illustration of the startup delay, assuming that the delay can be modeled by a first order time constant τ of about 40 seconds. It illustrates the influence of stoichiometric rate on the start up delay.

Since the output power remains low in the initialization state, an auxiliary

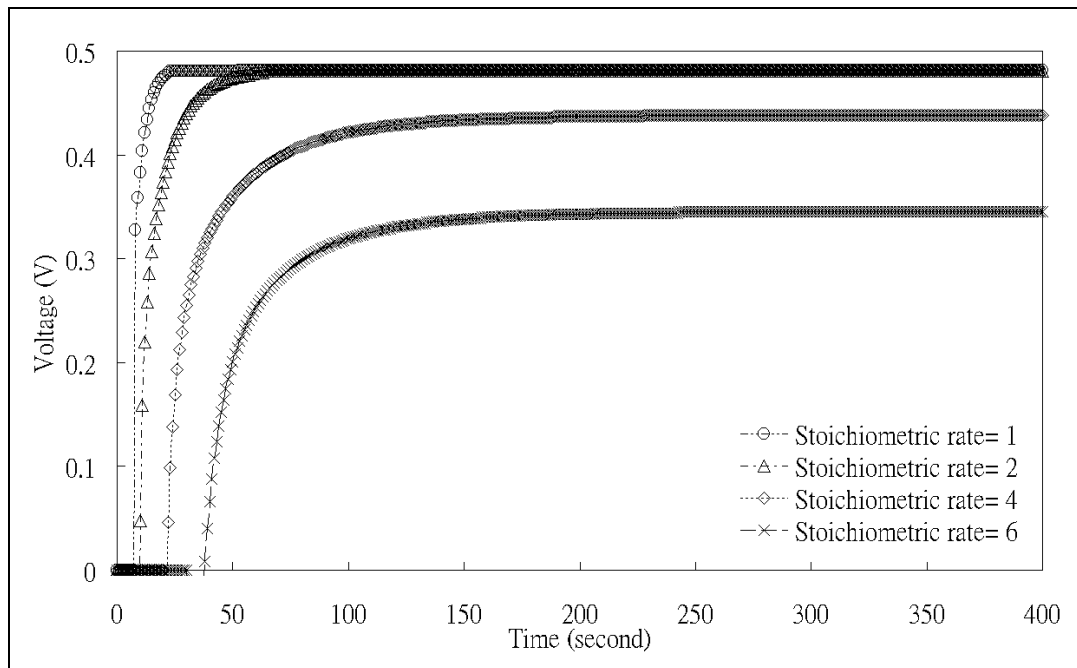


Figure 4.7: A quantitative illustration of the startup delay. Current density at $0.5\text{A}/\text{cm}^2$ and cell temperature at 70°C .

energy buffer, usually an additional battery, may be necessary to sustain the external loading. If this is the case, energy sinking in the initialization mode can be used to recharge the battery to reduce the loss.

4.6.2 Standby mode

As mentioned before, since the hydration of membrane remains low in startup, the fuel cell cannot produce the rated power at the very beginning of the operation. In order to shorten the time taken for the PEMFC to reach full-load operation, we suggest to add an auxiliary battery in the system. We may maintain the fuel cell in a periodically loaded condition even when the external loading is turned off. Using advanced power electronics, a bi-directional converter may be added to the system, so that the extra energy can be fed into the battery for recharging. This, however, requires the prediction of the external loading and intelligent control in the PEMFC unit. Since low load operation may cause dehydration in the fuel cell, an optimal operation point is also necessary. In this way, the time taken for then PEMFC to reach full-load operation can be shorten. This operational mode is particularly useful for fuel cell UPS where power failure is unacceptable.

4.6.3 Boost mode

In a PEMFC system, occasional overloading may be allowed. The transitional drop in voltage can be tackled by increasing the concentration of reactants. Consequently, by applying higher pressure in the cathode, the partial pressure of oxygen can be raised and eventually the cell voltage can be boosted. However, this procedure should not be continued for a long period of time. For high current rating, the membrane may be flooded or sometimes it may create some hot spots if the hydration of the membrane is uneven. This may result in permanent damage to the cell. Moreover, as seen in Figure 4.5, the heat loss is severe and the fuel efficiency is low under this mode of operation.

h

Chapter 5

Modeling and Simulation Using PSpice

The model presented in the previous chapter will be realized in Simulation Program with Integrated Circuit Emphasis (Spice). Spice is a standard tool for analog and mixed analog-digital simulation. It is a widely adopted simulation program in power electronics. A popular commercial version of Spice is PSpice, which allows a user to place and design their circuit on a drawing board prior to carrying out the analysis or circuit simulation. In this chapter, the fuel cell model will be implemented in PSpice's Capture CIS and presented in a schematic format. The corresponding netlist can also be found in the Appendix. Engineers, depends on their own preference, can reuse the information provided in this chapter in various versions of Spice available from different

developers.

5.1 Analogue behavior model

Analogue Behavior Model (ABM) provides a flexible descriptions of electronic components in terms of a transfer function or lookup table. This chapter will intensively use ABM as an implementation tool in the design. Different part of the system equations as described in chapter 4 will be modeled into a functional blocks by using ABM. This functional block shows how inputs are transformed into outputs in a more efficient way. Users can alter the values of input parameters in each of the functional block to fit their actual situation for simulation.

5.2 Preliminaries

The overall schematic is shown in Figure 5.1 and the corresponding net listing is given in the Appendix. As seen from Figure 5.1, each of the functional block is enclosed by a rectangular block in bold line. There are five functional blocks in total. Each of the functional block consists of certain ABMs. Depending on

the complexity of the subsystem, some of the functional blocks may contain more ABMs compared with others. To avoid unnecessary convergence problems, the use of division operation should be minimized in PSpice.

Even though ABM is a useful and efficient element in PSpice, it is not able to model the delay in time dimension. For the sake of this, simple analogue delay circuit was adopted in the design. It reflects the time delay in the system, such as the delayed response in the output voltage, dynamics of fuel consumption and heat release from the fuel cell system.

5.3 Spice Model

The Spice model in Figure 5.1 can be separated into 5 functional blocks including

1. Voltage losses in PEMFC operation
2. Energy used in pressurization
3. Reactant usage
4. Energy used in heat removal
5. Fuel cell output terminal

In next section, we are going to analysis each of this functional block individually. In each functional block, we will refer to the net listing provided in Appendix. Besides, Table 5.1 also provides a cross reference between the model presented in Chapter 4 and the model presented in PSpice. Theory of each formula has already been explained in Chapter 4 and will not be discussed in this chapter.

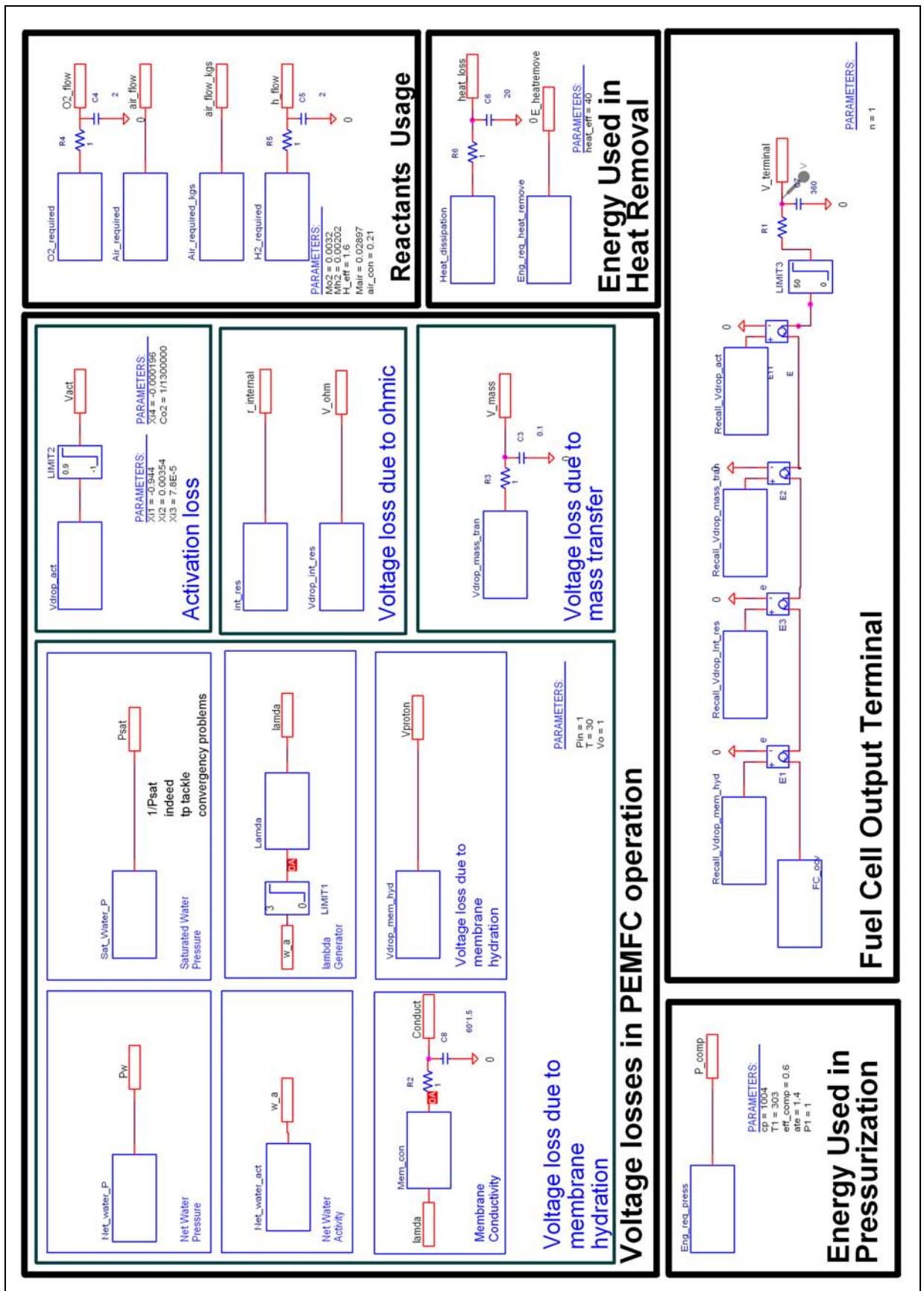


Figure 5.1: An illustration of PEMFC system model in PSpice.

ABM	PSpice Formulation	Output Physical Meaning	heritage	Equivalent in Electrochemical Model	Delay
Net_water_P	E_Net_water_P PW 0 VALUE (0.42*Pin)/(Vo+0.188)	Water vapor pressure (P_{vapor})	-	Eq. (4.14)	-
Sat_Water_P	E_Sat_Water_P PSAT 0 VALUE 1/PWR(10,(-2.1794+0.029537*T- 9.1837E-5*T*T+1.4454E-7*T*T*T))	Saturated vapor pressure (P_{sat})	-	Eq. (4.14)	60s
Net_Water_act	E_Net_Water_act W_A 0 VALUE V(Pw)*V(Psat)	Water vapor activity (a)	Net_water_P, Sat_Water_P	Eq. (4.15)	-
Lamda	E_Lamda LAMDA 0 VALUE If(V(N17116))=1,0.043+17.81*V(N17116) -39.85*V(N17116)*V(N17116) +36*PWR(V(N17116),3), V(N17116) *(14+1.4*(V(N17116)-1)))	Membrane hydration (λ)	Net_Water_act	Eq. (4.17), Eq. (4.18)	-
Mem_con	E_Mem_con CONDUCT 0 VALUE If(V(LAMDA))=1,1/((0.005139*V(LAMDA) 0.00326)*EXP(1268*(1/303- 1/(273+T))))),1/((0.005139*1- 0.00326)*EXP(1268*(1/303- 1/(273+T))))	Conductivity of the membrane (σ)	Lamda	Eq. (4.19)	-
Vdrop_mem_hyd	E_Vdrop_mem_hyd VPROTON 0 VALUE V(Ibat)*(V(Conduct))*0.001275	overpotential due to proton conductivity (η_{proton})	Mem_con	Eq. (4.20)	-
Vdrop_mass_tran	E_Vdrop_mass_tran V_MASS 0 VALUE 2.9*exp(PWR(3.2,-3)*(V(Ibat)*10))	Mass transfer effect	-	-	0.1 s
Vdrop_act	E_Vdrop_act N56635 0 VALUE Xi1+Xi2*(T+273)+Xi3*(T+273) *LOG(Co2)+Xi4*(T+273)*LOG(V(Ibat))	Activation overpotential (η_{act})	-	Eq. (4.2)	-
Int_res	E_Int_res R_INTERNAL 0 VALUE 0.01605-3.5*PWR(10,- 5)*(T+273)+8*PWR(10,-5)*V(Ibat)	Internal resistance of PEMFC ($R_{internal}$)	-	Eq. (4.4)	-
Vdrop_Int_res	E_Vdrop_Int_res V_OHM 0 VALUE V(r_internal)*V(Ibat)	Potential loss due to ohmic (η_{ohmic})	Int_res	Eq. (4.3)	-
O2_required	E_O2_required O2_FLOW 0 VALUE (Mo2*V(Ibat)/(4*96485))*5.4*(PWR(10,4))	Consumption of O ₂	-	Eq. (4.5)	2 s
Air_required	E_Air_required AIR_FLOW 0 VALUE (Mair*V(Ibat)/(4*96485))*(1/air.con)* Vo*5.4*(PWR(10,4))	Required air flow	O2_required	Eq. (4.6)	-
Air_required_kgs	E_required_kgs AIR_FLOW_KGS 0 VALUE (Mair*V(Ibat)/(4*96485))*(1/air.con)* Vo*(5.1*PWR(10,4))	Required air flow in kg/s	Air_required	-	-
H2_required	E_H2_required H_FLOW 0 VALUE (Mh2*V(Ibat)/(2*96485))* (1/0.084)*1000*H_eff	Flow rate of hydrogen	-	Eq. (4.5)	2 s

Table 5.1: Summary of AMBs and its relationship with electrochemical model

5.4 Voltage losses in PEMFC operation

This functional block consists of four sub-functional blocks, including:

- Voltage loss due to membrane hydration.
- Activation loss.
- Voltage loss due to ohmic.
- Voltage loss due to mass transfer.

These sub-functional blocks will be explained individually in coming section.

5.4.1 Voltage loss due to membrane hydration

Figure 5.2 illustrates the relationship and heritage of these ABMs in terms of functional block.

5.4.1.1 ABM - *Net_water*

ABM - *Vdrop_In_res* indicates how many water vapor is formed inside the PEMFC. It calculates the partial pressure of water vapor, P_{vapor} , using Eq. (4.5), Eq. (4.6), Eq. (4.8), Eq. (4.10), Eq. (4.11), Eq. (4.12), Eq. (4.13) and

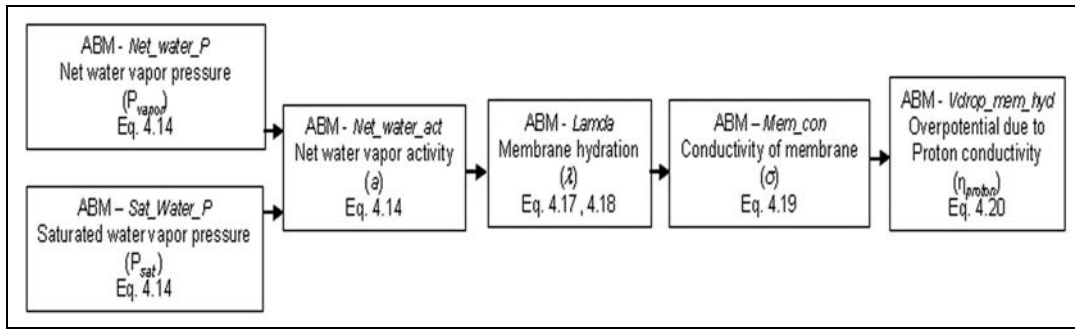


Figure 5.2: Illustration of the sub-functional block - voltage loss due to membrane conductivity in PSpice.

Eq. (4.14).

5.4.1.2 ABM - *Sat_water_P*

As mentioned in section 4.3.1, since saturated water vapor pressure changes in accordance with PEMFC operation temperature, ABM - *Sat_water_P* takes this effect into account. It calculates the saturated water vapor pressure, P_{sat} , at a specific operation temperature. This value is important in the following area.

5.4.1.3 ABM - *Net_water_act*

With the value of P_{vapor} and P_{sat} computed, it is now possible to find out the water vapor activity, a , in the PEMFC. Data of ABM - *Sat_water_P* and ABM - *Vdrop_In_res* then pass to the ABM - *Net_water_act*. Output of ABM - *Net_water_act*, a , reflects the water vapor activity. This value shows the amount of water form inside the PEMFC at a particular temperature.

5.4.1.4 ABM - *Lamda*

In the ABM - *Lamda*, the membrane hydration, λ , will be found based on the value of a . λ is a term used in electrochemistry, which implies how many water molecule is associated with each SO_3 . It is an intermediate value for the determination of the membrane conductivity due to water content. ABM - *Lamda* covers Eq. (4.17) and Eq. (4.18).

5.4.1.5 ABM - *Vdrop_mem_hyd*

Based on the value of λ from ABM - *Lamda*, the membrane conductivity is evaluated in the ABM - *Mem_con*. Finally the voltage drop due to membrane is calculated in ABM - *Vdrop_mem_hyd*. ABM - *Lamda* and ABM - *Vdrop_mem_hyd* covers Eq. (4.19) and Eq. (4.20) of previous chapter.

5.4.2 Voltage loss due to mass transfer

In many kinds of fuel cells, especially in low temperature fuel cells, the mass transfer effect is obvious. In the anode, the rate of transformation from hydrogen to proton is limited by the catalysis reactivity and reaction site etc. Thus, in the high current density region, current is limited, as the rate of transformation of hydrogen to proton is reaching its maximum. As a result, voltage drops rapidly in high current density region.

In the cathode, as oxygen is consumed, the concentration of the oxygen on the surface of the electrode decreases. In normal operation, oxygen will be quickly replenished by the circulating air. As current density increases, oxygen content circulating around the cathode may not be sufficient to replenish the consumed oxygen immediately. Thus the voltage of fuel cell drops significantly in high current density.

The effect of mass transfer is taken into account by the ABM20. This is a relatively simple model which evaluates the effect of mass transfer as a function of fuel cell current consumption with per-determined parameters.

5.4.3 Voltage loss due to activation

5.4.3.1 ABM - *Vdrop_act*

ξ_1 , ξ_2 , ξ_3 and ξ_4 correspond to ξ_1 , ξ_2 and ξ_3 of Eq. (4.2). They are pre-determined values. Besides, critical temperature, T_s , effective concentration of oxygen, Co_2 , and current density, I , are included in the ABM - *Vdrop_act*. The ABM - *Vdrop_act* implements Eq. (4.2).

The activation loss is determined by both the loading current and operation temperature. As mentioned in section 2.5.2, it is due to the kinetic barrier at the very beginning of reaction. Nevertheless, the drop of voltage in ABM - *Vdrop_act* simulates the dramatically drop of fuel cell voltage at low current density region.

5.4.4 Voltage loss due to ohmic

5.4.4.1 ABM - *Int_res*

Ohmic loss is sensitive to the temperature. The ABM - *Int_res* calculates the purely internal resistance of the fuel cell. This value is sensitive to the operation temperature of the fuel cell. Besides, parameters of the ABM25 may change in accordance with the materials used in fuel cell construction.

The ABM25 simulates Eq. (4.3).

5.4.4.2 ABM - *Vdrop_In_res*

Output of ABM - *Int_res* is passed to ABM - *Vdrop_In_res* to evaluate the exact voltage drop due to ohmic loss. The ABM - *Vdrop_In_res* simulates Eq. (4.4).

5.5 Fuel cell output terminal

This part mainly combines the potential losses of the fuel cell. It includes losses due to membrane hydration, mass transfer, activation and purely ohmic resistance. All the considerations in section 5.4.1, 5.4.2, 5.4.3 and 5.4.4 are summed up in this functional block. This functional block simulates the output terminals of a complete self humidified fuel cell.

In the output terminal, the user can trace the variation of the battery terminal output voltage. For converter designer, the DC/DC converter can be connected to this output terminals. This block covers Eq. (4.1) and also includes additional information regarding mass transfer effect.

5.6 Reactants Usage

To simulate the reactants usage, as illustrated in Figure 5.3, four ABMs are included. They calculate the flow rate of oxygen, air and hydrogen.

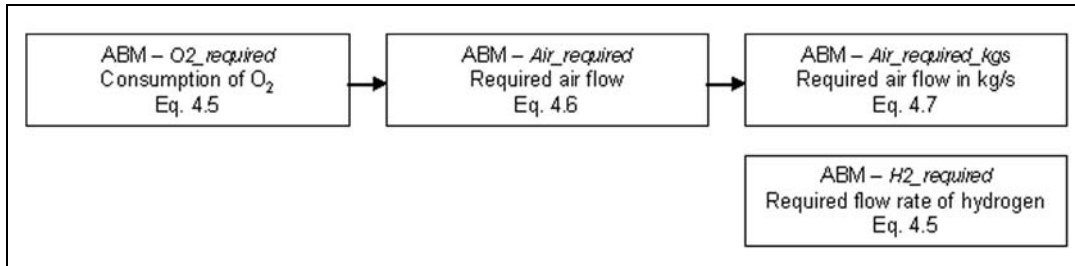


Figure 5.3: Illustration of fuel consumption in PSpice.

5.6.0.3 ABM - *O2_required*

ABM - *O2_required* calculates the minimum amount of oxygen needed, based on current consumption. It contains the functional description of Eq. (4.5).

5.6.0.4 ABM - *Air_required*

In most applications, oxygen is supplied from ambient. The output of ABM - *O2_required* (consumption of O_2) will pass to ABM - *Air_required*. ABM - *Air_required* will evaluate the necessary flow rate of air to replenish the corre-

sponding oxygen consumption.

5.6.0.5 ABM - *Air_required_kgs*

Finally, in ABM - *Air_required_kgs*, flow rate of air will be converted into standard unit.

5.6.0.6 ABM - *H2_required*

ABM - *H2_required* calculates the flow rate of hydrogen in accordance with Eq. (4.6). Noted that, the flow rate of hydrogen depends on the hydrogen efficiency. As usual, this value is approximately 1.6. That means 1.6 times of minimum hydrogen is required.

This functional block mainly provides additional information to the designer to gain information on fuel consumption, especially the hydrogen usage. Results generated from this block are useful for designers who are concerned with the long term operation, e.g., in uninterrupted power supplies (UPS).

The details of each of the functional block have now been explained. In the next section, the PSpice simulation results will be presented.

5.7 Simulation results

5.7.1 Voltage versus current characteristic

A simulated voltage versus current characteristic of a typical PEMFC can be seen in Figure 5.4. It can be decomposed into three regions including the ohmic loss region, activation overpotential region and the mass transfer effect region.

The activation overpotential dominates at low current density as there is no sufficient energy for the proton to overcome the kinetic barrier. However, these losses becoming insignificant as current increases up to $20\text{mA}/\text{cm}^2$.

In medium current density region, most of the energy is lost in the ohmic polarization. The loss in ohmic remains constant in the medium current density region. Thus, the drop in voltage maintains steady.

Finally, voltage drops dramatically as a result of the mass transfer effect. The rate of transformation of hydrogen to proton is up to its limited. Therefore, the voltage collapsed.

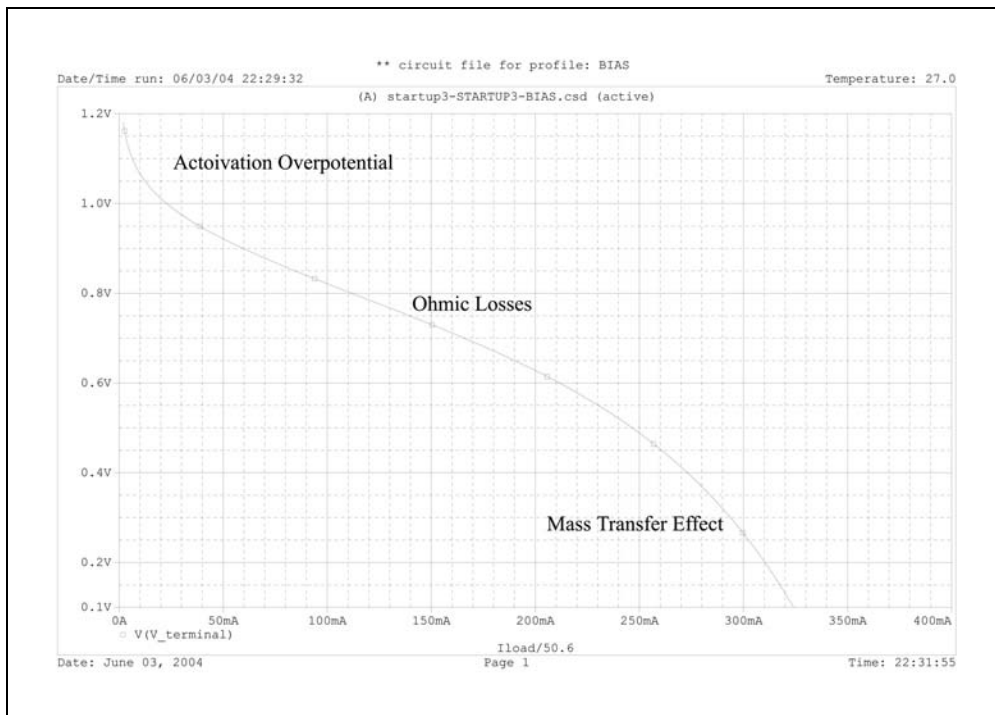


Figure 5.4: A typical voltage versus current characteristic of a PEMFC in PSpice simulation with pressure in cathode = 1 bar, operation temperature at 60 °C and stoichiometric rate = 2.

5.7.2 Fuel cell operation characteristics

Based on the model presented, a number of simulations on the operational characteristics of a typical PEMFC have been carried out. Figure 5.5 shows the performance of PEMFC under different operation pressure. Figure 5.6 illustrates the variation due to change in air flow rate. In Figure 5.7 indicates the startup delay in PEMFC. The startup delay has a correlation with air flow in cathode.

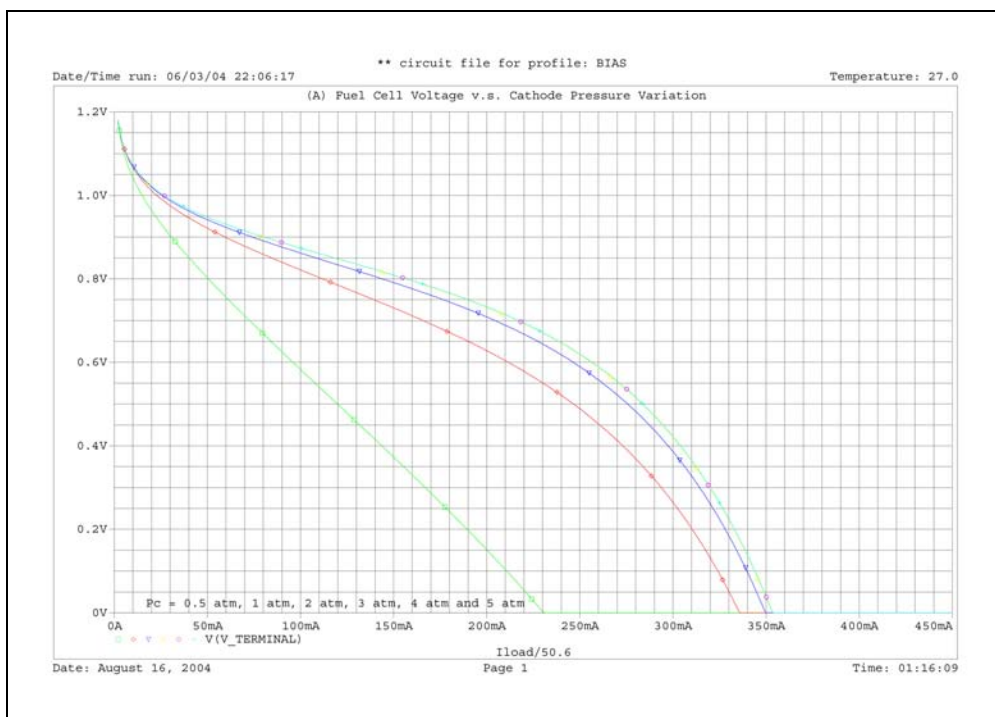


Figure 5.5: Effect on pressurization in PSpice simulation with temperature at 60 °C and stoichiometric rate = 2. Pressure at cathode = 0.5 bar (□), 1 bar (◇), 2 bar (▽), 3 bar (△), 4 bar (◇) and 5 bar (+).

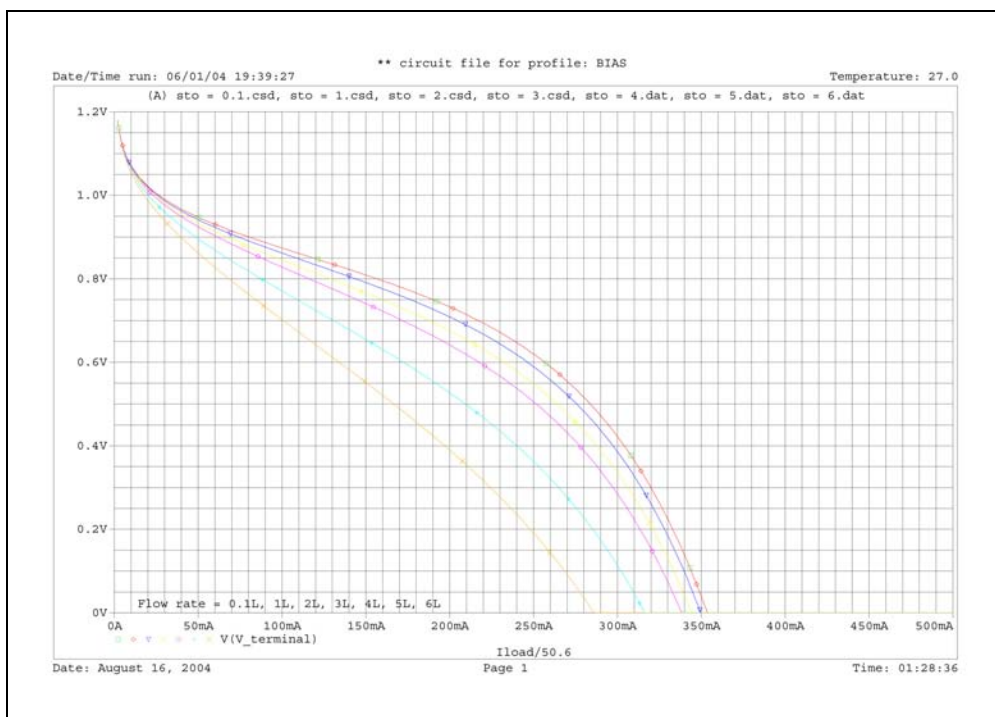


Figure 5.6: Effect on stoichiometric rate effect in PSpice simulation with operation temperature at 60 °C and cathode pressure = 1 bar. Stoichiometric rate = 0.1 (□), 1 (◇), 2 (▽), 3 (), 4 (◇), 5 (+) and 6 (×)

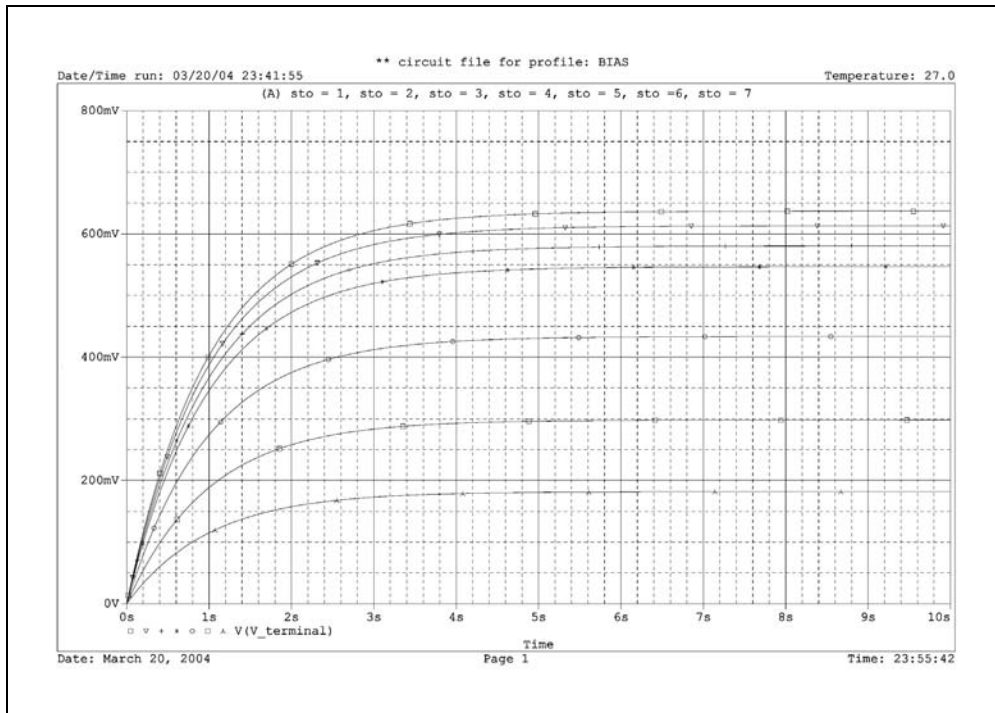


Figure 5.7: Startup effect in PSpice simulation with operation temperature at $60\text{ }^{\circ}\text{C}$, cathode pressure = 1 bar with current consumption of $0.2\text{A}/\text{cm}^2$. Stoichiometric rate = 1, 2, 3, 4, 5, 6 and 7.

5.7.3 Fuel usage

Figure 5.8 shows the performance of PEMFC with different reactant flow rates in the cathode. Here, in our case, the stoichiometric rate of air is set to two, so as to lower the effect of mass transfer effect at high current density.

Figure 5.9 indicates the required flow rate of hydrogen in liter/minute. Here, it is assumed that an R-size cylinder is used for hydrogen supply. The current density is set as $0.2\text{A}/\text{cm}^2$. A fuel cell with electrode area of 27cm^2 is used. The cell has total 5.4A output current with 0.625V output voltage in accordance with simulation result of Figure 5.4.

Now, assume that the simulated fuel cell has an output power of 3.38W with $54\text{mL}/\text{min}$ flow of hydrogen. In normal situation, an R-size cylinder carrying 3600m^3 of hydrogen. Therefore, the simulated fuel cell can have 1111 hours of operation time. With this information, engineers can approximate the life time of a standby power delivered by a particular PEMFC system.

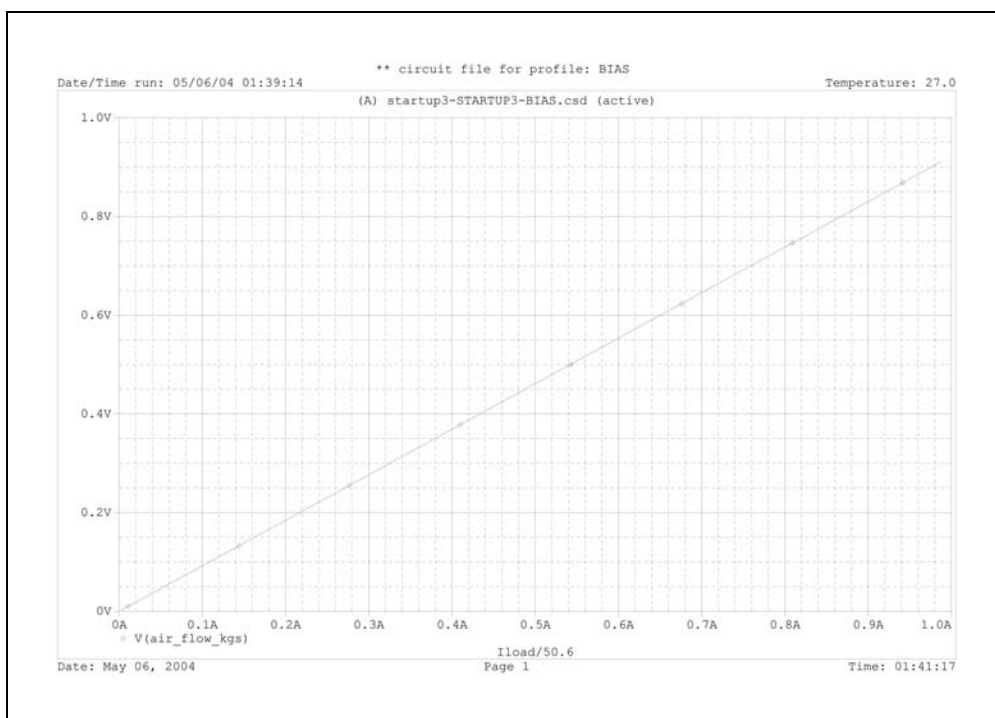


Figure 5.8: Air consumption (liter/minute) in PSpice simulation with operation temperature at 60 °C, cathode pressure = 1 bar and stoichiometric rate = 2. X-axis indicates current density in A/cm², Y-axis indicates flow rate of air in liter/min.

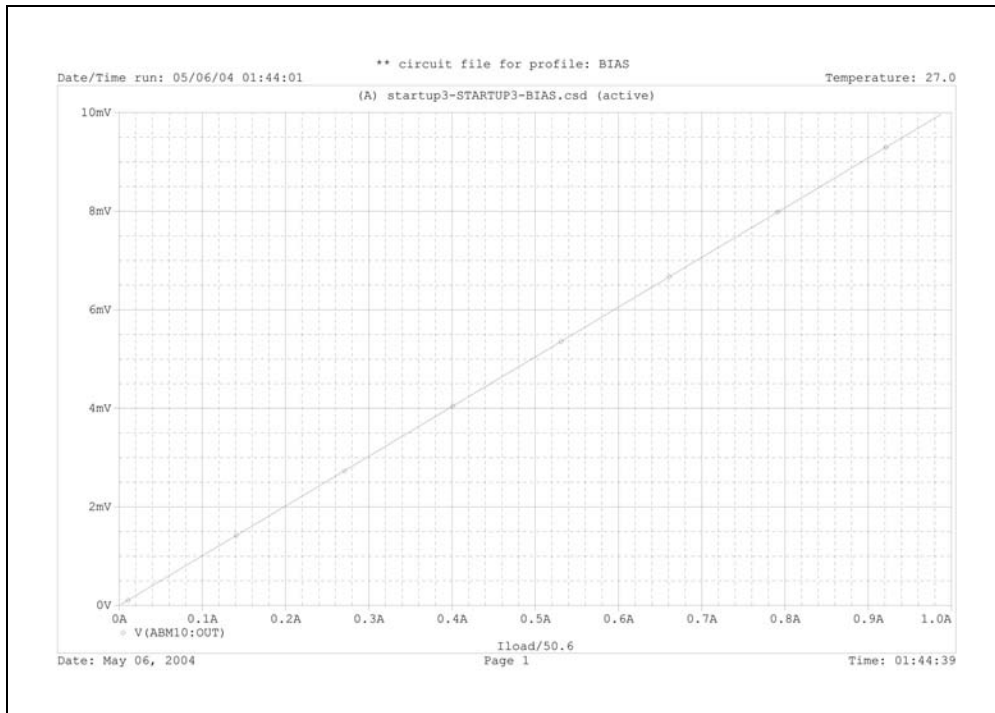


Figure 5.9: Hydrogen consumption in PSpice simulation with operation temperature at 60 °C, cathode pressure = 1 bar and stoichiometric rate = 2. X-axis indicates current density in A/cm², Y-axis indicates flow rate of hydrogen in liter/min.

5.7.4 Application of the PSpice model in UPS system

In a PEMFC powered UPS system, it is important to consider the time taken for the PEMFC to startup. The following calculation example is based on the simulation results from the PSpice model .

Assuming that the UPS under design will be used to backup the operation of a mainframe computer. The required power for this mainframe computer is 400W.

Assume that the inverter can achieve 85% conversion efficiency. Therefore, the output power of the PEMFC will be at least 520W.

According to Figure 5.5, we set the operation point of the PEMFC at $0.2A/cm^2$. From the figure, the PEMFC is capable to delivery 0.625V at the output terminal.

For example, if we select the output of the PEMFC to be 24V, the required PEMFC will consist of 38 cells in stack. In order to achieve the required current rating, the PEMFC should have a electrode size of $100cm^2$.

Assume that the initial hydration of the PEMFC is behaved as shown in Figure 5.7. If the stoichiometric rate is kept at 2, the PEMFC will become stable in 6 seconds.

Assume that a 24V lead acid battery is adopted in the system and that the lead acid battery is able to supply a current up to 5C level. The size of the lead acid battery will be at least 5Ah including the power required for the PEMFC startup. It is also important to inspect the loading characteristic of the lead acid battery to ensure a stable output at continuous 5C level loading.

5.8 Conclusion

This chapter demonstrates a successful modeling of the developed fuel cell model into PSpice. Crucial simulation results such as voltage against current characteristic, pressurization effect, stoichiometric rate effect and fuel consumption have been presented.

Modeling and simulation help power converter designers to actually predict the performance of PEMFC without going into the details of electrochemistry. With the integrated model in PSpice, electronic engineers can have an idea of

how the fuel cell performs under various conditions.

This model developed is expected to provide a channel for converter designers to understand the characteristic of PEMFC. With the availability of this model, designers can optimize not only the electronic circuit but also the overall system design.

Chapter 6

Evaluation of Model

This chapter will cover the evaluation of the PSpice model developed in previous chapter. It includes the comparison of voltage against current characteristic, pressurization effect, stoichiometric rate, startup delay with experimental results.

6.1 Voltage Characteristic

Figure 6.1 shows a simulation result of voltage against current characteristic from the PSpice model. It simulates the effect of activation overpotential, ohmic losses, proton conductivity and mass transfer. In comparison, Figure 6.2 shows an experimental result under the same operation condition.

Referring to Figure 6.2, a dramatical drop of voltage can be observed at the low current density region due to the effect of activation overpotential. In medium current density region, the drop of voltage is relative linear since most of the drop in voltage is contributed by the constant ohmic loss in the PEMFC. As current increases, voltage drops rapidly when the mass transfer effect appears.

With regard to the simulation result in Figure 6.1, the PSpice model can approximate the shape of the PEMFC loading characteristic. However, in high current density region, the PSpice model is not sufficiently good to simulate the drop of voltage due to mass transfer.

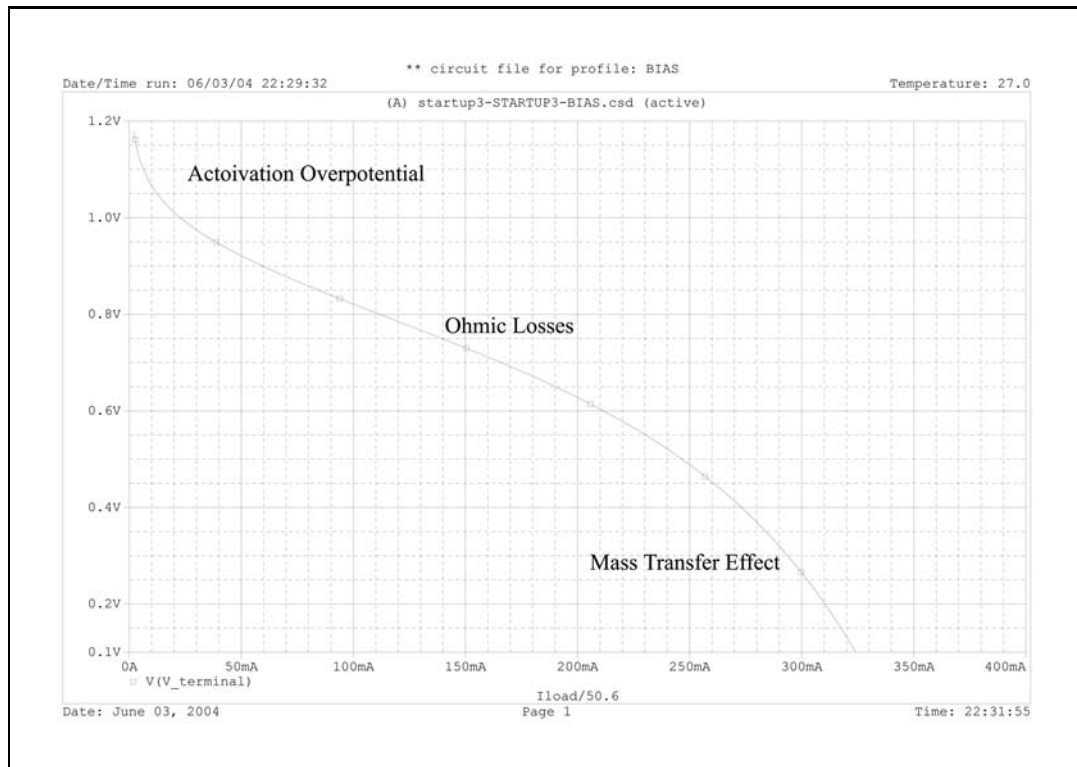


Figure 6.1: Voltage against current characteristics in PSpice simulation with operation temperature at 60°C , cathode pressure = 1 bar and stoichiometric rate = 2.

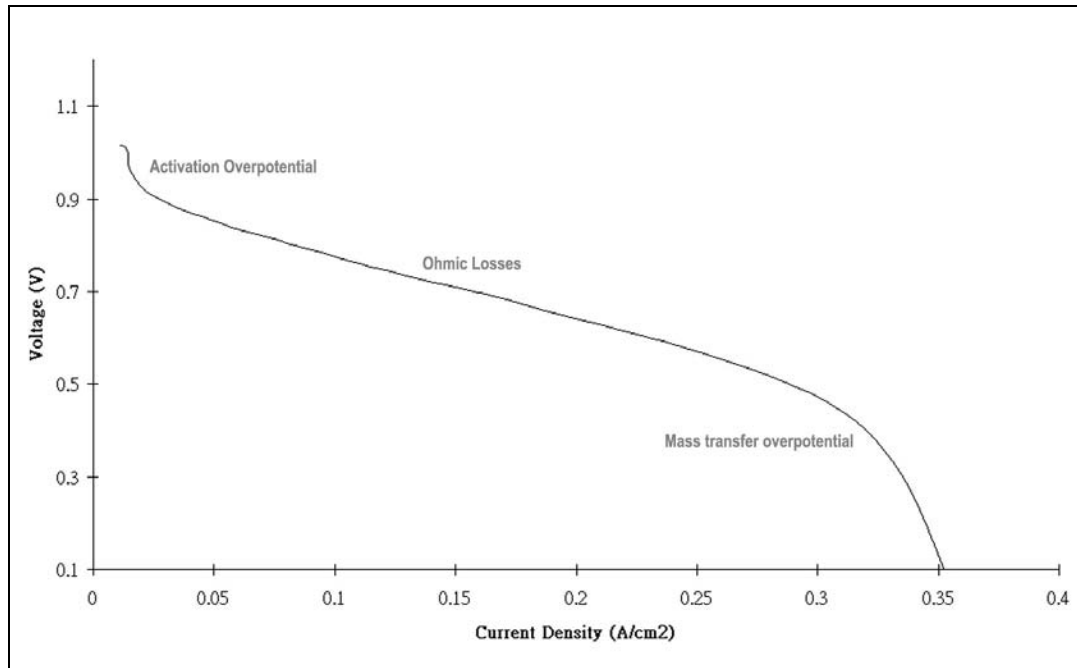


Figure 6.2: Experimental result of voltage against current characteristics with cathode pressure = 1 bar and air flow of 0.8L/min.

6.2 Pressurization effect

Figure 6.3 illustrates an experimental result of the PEMFC voltage against variation in cathode pressure. The pressure in the cathode was controlled while the flow of air was maintained to be the same along each examination.

It can be observed that, agreeing with the PSpice model, at a pressure level lower than 1 atm, the power output from the PEMFC is significantly lower. This effect can also be reflected from the PSpice model as seen in Figure 6.4.

However, as current density increases, the level of improvement due to pressurization in experimental result cannot be totally reflected in the PSpice model. In accordance with the PEMFC structure and materials used, the parameters involved in the model should be calibrated each time in order to obtain the optimal simulation result. Since these parameters have not been specifically computed, the level of the significance of pressurization cannot be totally reflected in the PSpice model. In addition, mass transfer effect is another factor that makes the simulation slightly different from experimental result. It is because a relative simple model is used to simulate the effect of mass transfer. This inadequacy becomes observable as the current density increases.

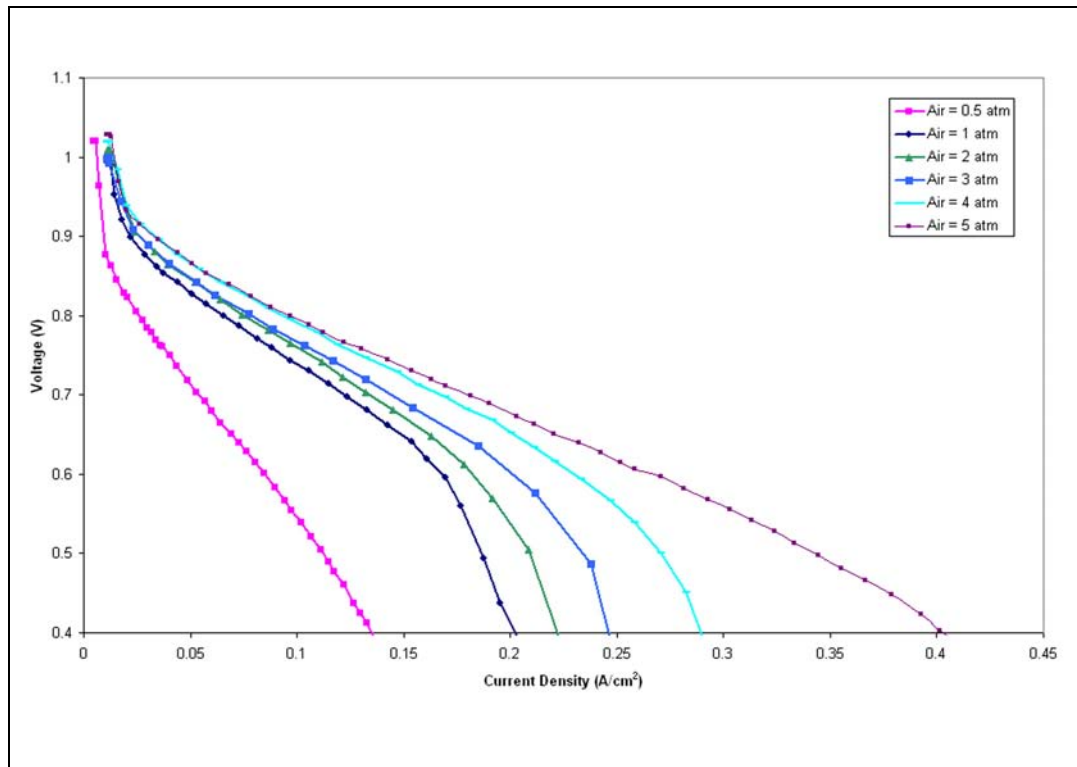


Figure 6.3: Experimental result on pressurization with stoichiometric rate = 2. Pressure at cathode = 0.5 bar, 1 bar, 2 bar, 3 bar, 4 bar and 5 bar.

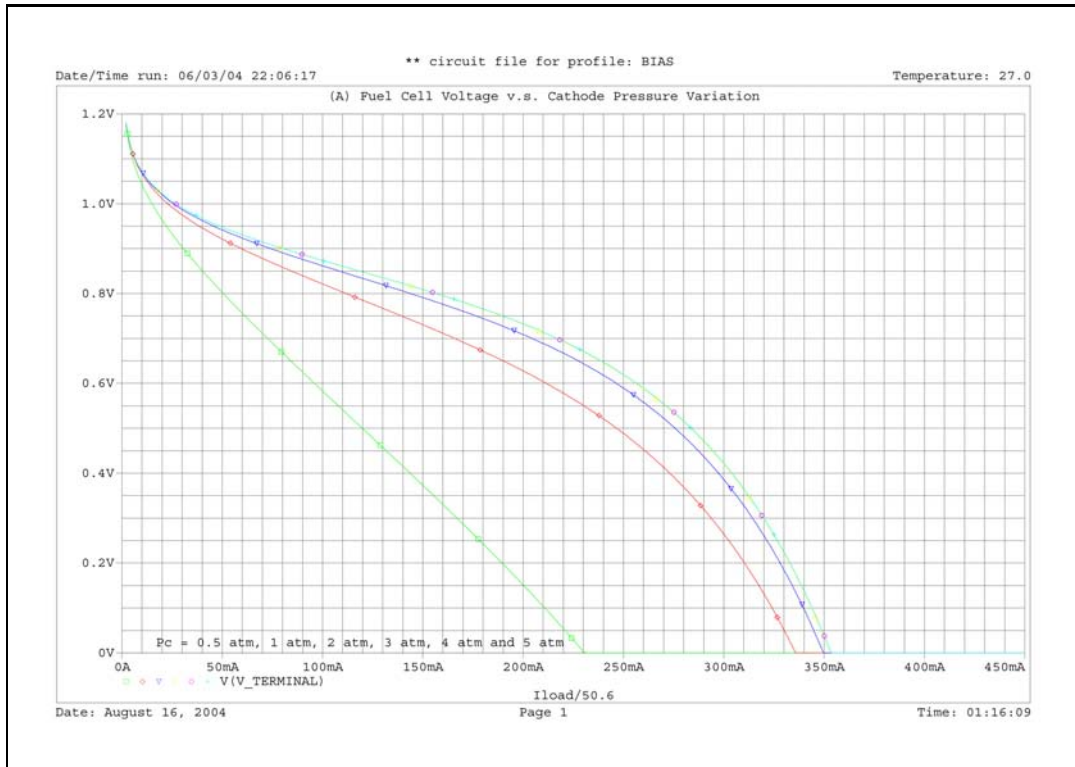


Figure 6.4: Effect on pressurization in PSpice simulation with temperature at 60 °C and stoichiometric rate = 2. Pressure at cathode = 0.5 bar (□), 1 bar (◇), 2 bar (▽), 3 bar (△), 4 bar (◇) and 5 bar (+).

6.3 Stoichiometric Rate Effect

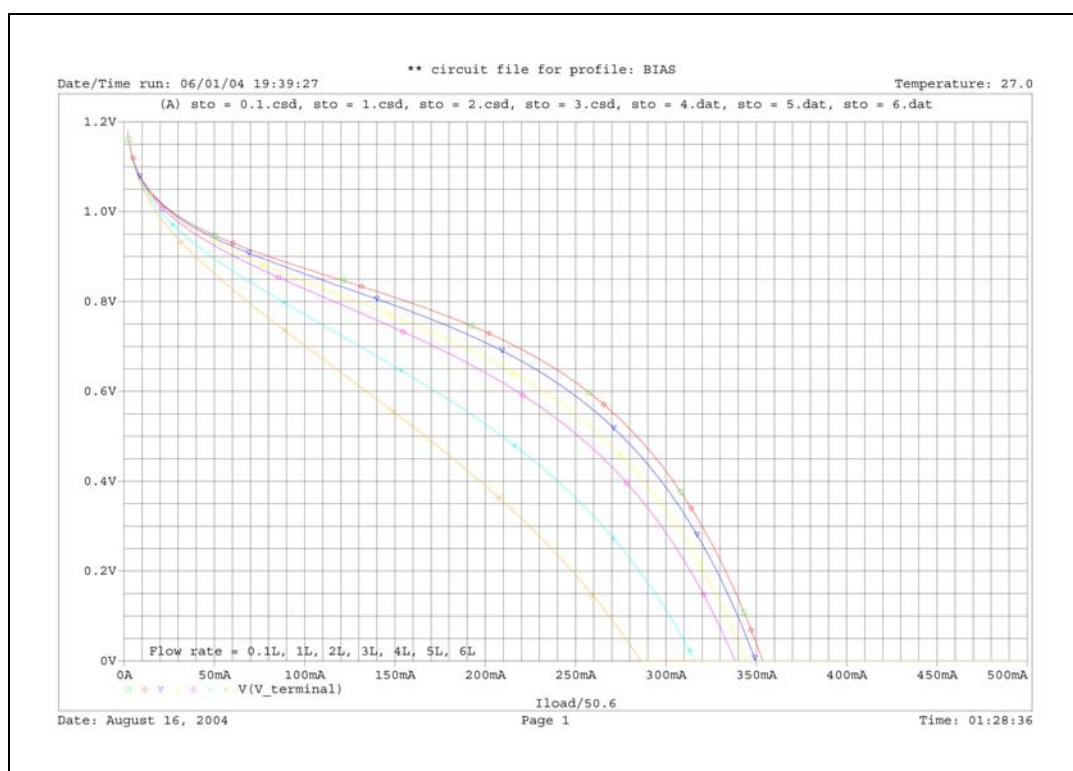


Figure 6.5: Effect on stoichiometric rate in PSPICE simulation with operation temperature at 60 °C and cathode pressure = 1 bar. Stoichiometric rate = 0.1 (□), 1 (◇), 2 (▽), 3 (), 4 (◊), 5 (+) and 6 (×)

Figure 6.5 illustrates a PSpice simulation result of a PEMFC with controlled fuel flow in cathode. In accordance with the simulation result as seen in Figure 6.5, the voltage of the PEMFC decreases as flow rate of air increases. It is mainly due to the fact that dehydration effect of the membrane becomes severe as air flow increases.

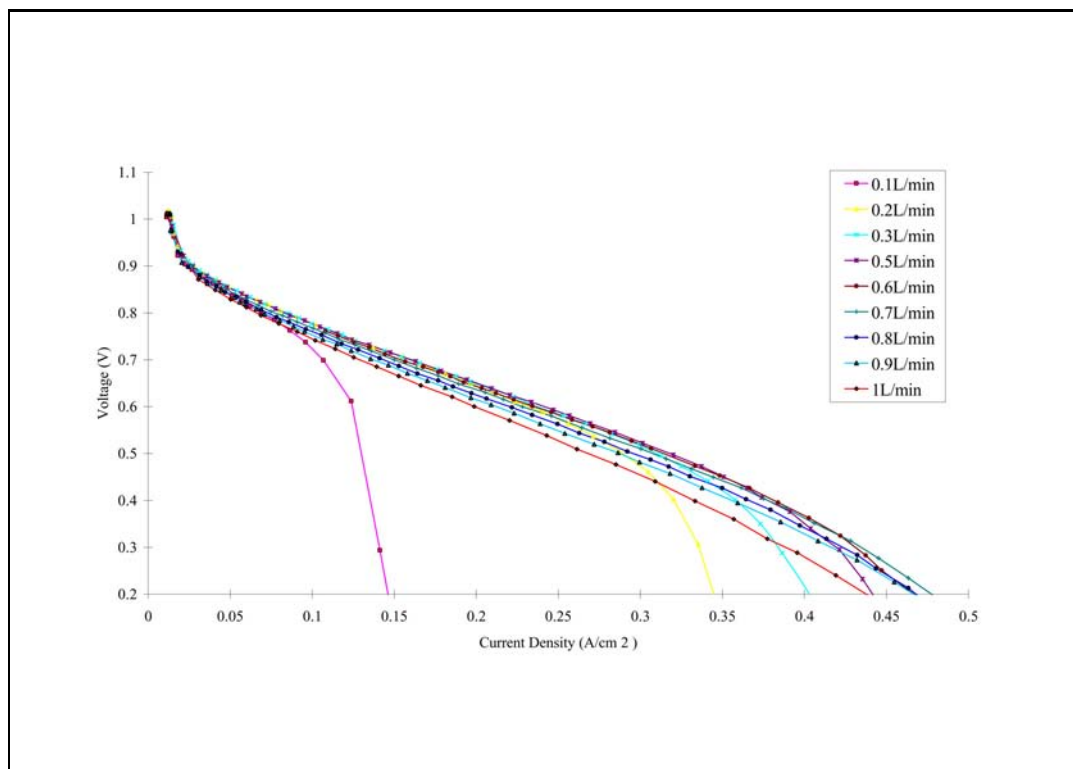


Figure 6.6: Experimental result on stoichiometric rate with cathode pressure = 1 bar. Air flow in cathode = 0.1L/min, 0.2L/min, 0.3L/min, 0.4L/min, 0.5L/min, 0.6L/min, 0.7L/min, 0.8L/min, 0.9L/min and 1L/min

However, as seen from the experimental result in Figure 6.6, when the flow rate of air increases from 0.1L/min, output voltage increases. This effect is even more significant in the high current density region.

Though, starting from 0.8L/min, this marginal effect can no longer be obtained. On the contrary, voltage reduces as the flow of air further increases. Therefore, there must be a threshold where the improvement of mass transfer effect can no longer compensates the dehydration effect in the membrane. In the experiment, the current sweep is preformed in one minute and voltage was logged by a computer through the digital oscilloscope. Therefore, the long term effect of the dehydration is not completely disclosed in the experiment data. As a result, the improvement of mass transfer effect dominates in the experiment, while the effect due to dehydration of membrane is invisible. Therefore, the deviation between simulation result and experimental fact can be explained.

In fact, the performance of PEMFC deteriorates from 0.8L/min onward which confirms that excessive flow of air is not completely beneficial for PEMFC operation, especially in continuous operation. It also confirms with our model that excessive flow of air will decrease the proton conductivity. Therefore

the reactant flow rate in cathode should be carefully controlled, so that the mass transfer effect can be reasonably minimized and the air flowing into the PEMFC is not drying the membrane.

In the experiment, the flow rate of air is maintained constant throughout the whole sweep of the current. Therefore, even though oxygen appears to be abundant in low the current density region, as current density increases, the mass transfer effect becomes obvious. However, in the simulation, the flow rate of air is computed in such a way that it is always twice the minimum needed. The stoichiometry rate is set at 2. Therefore, the variation between experiment and simulation results can be explained.

6.4 Startup delay

Figure 6.7 illustrates an experimental startup delay of a PEMFC with current loading of $0.1\text{A}/\text{cm}^2$. The PEMFC under test had been idle for nearly four months in normal room temperature. $0.1\text{L}/\text{min}$ of air was applied to prevent the possibility for further dehydration of PEMFC. The voltage was logged by a computer through a digital oscilloscope. The PEMFC voltage is back to a stable state in 30 minutes. A first order time constant is adopted into the PSpice model and shown in Figure 6.8.

This type of startup delay is caused by the low proton conductivity in the membrane. The delay is introduced as a result of the time taken for the water to be generated internally. In fact, the exact delay time is difficult to model, because the level of hydration of fuel cell with respect to time is not easy to predict. As usual, a regularly operating fuel cell can have startup delay from 2 minutes to 15 minutes. The delay time is also related to the cell structure and storage condition.

As seen from Figure 6.7 and Figure 6.8, the model is sufficiently accurate to approximate the startup response.

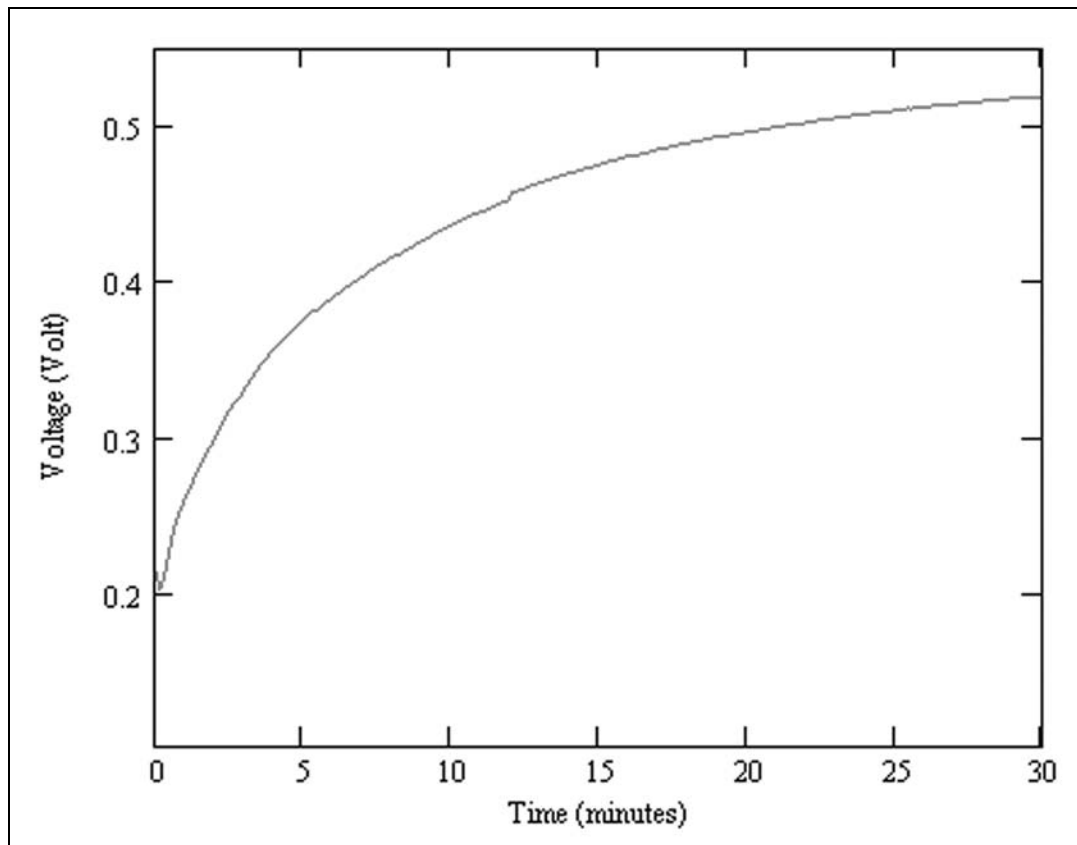


Figure 6.7: Experimental startup delay

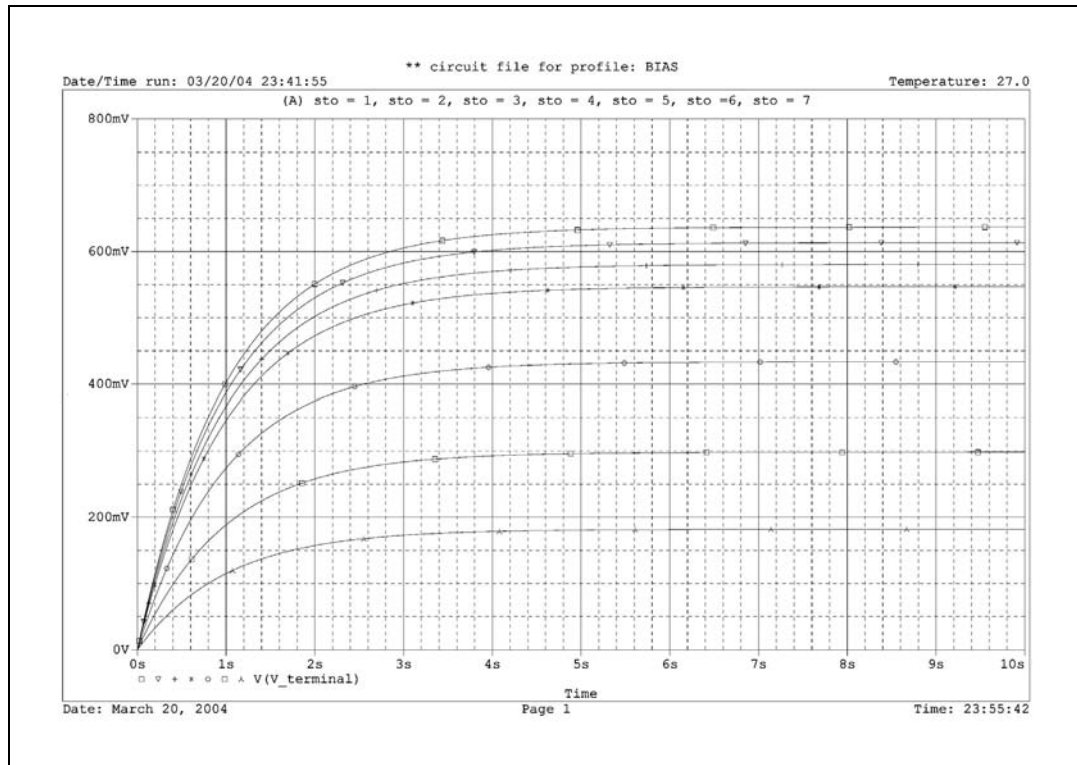


Figure 6.8: Startup delay of PEMFC in PSpice simulation

Chapter 7

Conclusion

7.1 Summary of original result

In this thesis, we go through the fundamental operation principle of fuel cell and the significance of fuel cell technology in comparison with conventional energy sources. Different types of fuel cells and their characteristics are introduced. Among them, the proton exchange membrane fuel cell (PEMFC) is particularly chosen to be further analyzed .

The inner structure of PEMFC, including membrane, electrodes, electrocatalyst, bi-polar plate and electrode membrane assembly (MEA) was studied. With regarding to each component, the function, existing status and advancements were reported.

From the system point of view, a complete PEMFC system was investigated. The system includes a fuel processor, an air management sub-system, a water management sub-system, a thermal management sub-system and a power conditioner.

Based on the a self humidified PEMFC system, a model was developed. It covers the effects due to activation overpotential, ohmic loss, proton conductivity and mass transfer. In addition, a number of operation modes are suggested. The proposed operation modes can satisfy different applications. For instance, the initialization mode can shorten the startup period of an uninterrupted power supplies (UPS); the boost mode can provide extra power for electric vehicle in acceleration; the standby mode can preserve the water inside the fuel cell in idle state.

Water management is of the most important issues in a PEMFC system. In the model, a simplified model governs proton conductivity is specially derived. It approximates the effect of membrane hydration. By this feature, we can study the variation of PEMFC performance due to changes in dehydration of membrane, stoichiometric rate and mass transfer effect.

The model is further integrated into Simulation Program with Integrated Circuit Emphasis (Spice). It extends the usage of the model to power electronics. On top of the information given previously, the PSpice model also provides supplementary information such as reactants usage, energy used in heat removal and energy used in pressurization. Most important, electronic engineers can now have an easier starting point to begin their fuel cell project, without involving too much into fuel cell fundamental theories.

7.2 Further Extension

7.2.1 Improving accuracy in modeling mass transfer effect

In order to increase the accuracy of the model, it is highly desirable to improve the model of mass transfer. Since air is used in the cathode, the effect due to mass transfer is highly dependent on the flow rate and the concentration of oxygen in the air. Also, since a relatively simple model is adopted in this thesis, the deviation of the model becomes noticeable in the high current density region. Additional elements can be added to better simulate the dynamic responses of the fuel cell. For example, the diffusion coefficients of oxygen at

different stages, $D_{O_2}^{eff}$, as presented by Baschuk et al.[34], play an important role in modelling the mass transfer effect. However, an intensive computational effort is required to evaluate the the specific $D_{O_2}^{eff}$ along each interface because the MEA of PEMFC consists of many materials, the specific value of $D_{O_2}^{eff}$ along each interface is different.

7.2.2 System optimization

It is interesting to see that power of the fuel cell increases as the air pressure is increased in cathode. Meanwhile, it is also found that an increase in air flow can improve the performance of fuel cell under certain conditions. In practice, assuming that an equal amount of energy is used in pressurization, reducing the outlet of air can reduce the flow rate of air while achieving higher system pressure. Therefore, it would be interesting to explore the relationships among the output power, flow of air and pressure in the system. By doing so, we can find an optimal point of operation, so that the lowest power is used in pressurization while minimizing the effect due to mass transfer.

7.2.3 Laplace Sources

The ELaplace source in PSpice can be used to model a complex systems or a control system. It has a voltage or current source as its input and produces an output based on a transfer function defined in the Laplace domain. Although the ELaplace source is usually used in frequency domain, it can also be used for modeling in time domain.

For example, regarding the PSpice model illustrated in Figure 5.1, the simple first order delay used in *ABM - Mem_con* can be replaced by an ELaplace with a transfer function of :

$$H(s) = \frac{1}{1+sR_2 \cdot C_8}$$

It is therefore feasible to replace the simple RC delay circuit in PSpice by an ELaplace model. The major advantage is that designers can change the time constant explicitly rather than the RC circuit. However, compared with a simple RC circuit, an ELaplace source may take more computation power.

Appendix A

A.1 .cir simulation file for PSpice

```
* source STARTUP3
E_LIMIT2 VACT 0 VALUE LIMIT(V(N56635),-1,0.9)
E_Sat_Water_P PSAT 0 VALUE 1/PWR(10,(-2.1794+0.029537*T-9.1837E-5*
+ T*T+1.4454E-7*T*T*T))
E_LIMIT1 N17116 0 VALUE LIMIT(V(W_A),0,3)
E_ABM11 N68555 0 VALUE
+ If(V(LAMDA)i=1,1/((0.005139*V(LAMDA)-0.00326)*EXP(1268*(1/303-1/(273+
+ T))))),1/((0.005139*1-0.00326)*EXP(1268*(1/303-1/(273+T))))))
E_Eng_req_heat_remove E_HEATREMOVE 0 VALUE V(heat_loss)/heat_eff
+
E_E1 N28866 N04115 N00151 0 1
H_H1 IBAT 0 V_HH11
V_H_H1 N3077300V
E_E2 N38788 N80456 N5398901
E_O2_required N2750500V ALUE( + Mo2 * V(Ibat)/(4 * 96485)) * 5.4 * (PWR(10, 4))
C_C30V_MASS 0.1
C_C50H_FLOW 2
E_Vdrop_mem_hyd V_PROTON 0V ALUE V(Ibat) * (V(Conduct)) * 0.001275
E_Recall_Vdrop_mem_hyd N001510V ALUE -V(Vproton) * n
R_R1 N81360V_TERMINAL 1
E_Net_water_PPW 0V ALUE (0.42 * Pin)/(Vo + 0.188)
E_int_res R_INTERNAL 0V ALUE 0.01605 - 3.5 * PWR(10, -5) * (+ T + 273) + 8 * PWR(10, -5) * V(Ibat)
E_ABM18 N632260V ALUE Iload
E_Air_required AIR_FLOW 0V ALUE (Mair * V(Ibat)/(4 * 96485)) * (1/ + air_con) * Vo * 5.4 * (PWR(10, 4))
R_R2 N68555 CONDUCT 1
```

```

E_Vdrop_actN566350V ALUEXi1 + Xi2 * (T + 273) + Xi3 * (T + 273) * LOG( + Co2) + Xi4 * (T + 273) * LOG(V(Ibat))
R_R6N72169HEAT_LOSS1
R_R3N377410V _MASS1
E_Eng_req_pressP_COMP0V ALUEcp * (T1/eff_comp) * (PWR((Pin/ + P1), 0.286) - 1) * V(air_flow_kgs)
E_Vdrop_int_resV_OHM0V ALUEV(r_internal) * V(Ibat)
E_E11N80456N81924N8056701
R_R5N276940H_FLOW1
E_LIMIT3N813600V ALUELIMIT(V(N81924), 0, 50)
E_Lamda LAMDA 0 VALUE If(V(N17116))=1,0.043+17.81*V(N17116)
+ -39.85*V(N17116)*V(N17116)+36*PWR(V(N17116),3),V(N17116)*(14+1.4*(V(N17116)-1)))
+
E_Recall_Vdrop_Int_resN040700V ALUEV(V_ohm) * n
E_ABM19N317710V ALUEV(V_terminal)
E_Vdrop_mass_tranN3774100V ALUE2.9 * exp(PWR(3.2, -3) * (V(Ibat) * 10))+
R_R4N275050O2_FLOW1
E_FC_ocuN288660V ALUE0.8 * n
C_C80CONDUCT360
E_Air_required_kgsAIR_FLOW_KGS0V ALUE( + Mair * V(Ibat)/(4 * 96485)) * (1/air_con) * Vo * (5.1 * PWR(10, 4))
E_Recall_Vdrop_actN805670V ALUE - V(Vact) * n
C_C70V_TERMINAL360
E_Net_water_actW_A0V ALUEV(Pw) * V(Psat)
G_G4N31771N30773N6322601
E_E3N04115N38788N0407001
C_C60HEAT_LOSS20
E_Heat_dissipationN721690V ALUEV(V_ohm) * n * V(Ibat)
E_H2_requiredN2769400V ALUE( + Mh2 * V(Ibat)/(2 * 96485)) * (1/0.084) * 1000 * H_eff
C_C40O2_FLOW2
E_Recall_Vdrop_mass_tranN539890V ALUEV(V_mass) * n/1000
.PARAMXi3 = 7.8E - 5Pin = 1Xi4 = -0.000196P1 = 1Co2 = 1/1300000Mh2 = 0.00202FanV = 5
+ Vo = 10n = 1sto = 0H_eff = 1.6air_con = 0.21Iload = 10Mair = 0.02897eff_comp = 0.6
+ cp = 1004heat_eff = 40ate = 1.4A = 50.6PumpV = 12Xi1 = -0.944Xi2 = 0.00354T1 = 303
+ T = 30Mo2 = 0.0032

```


A.2 MathCad simulation

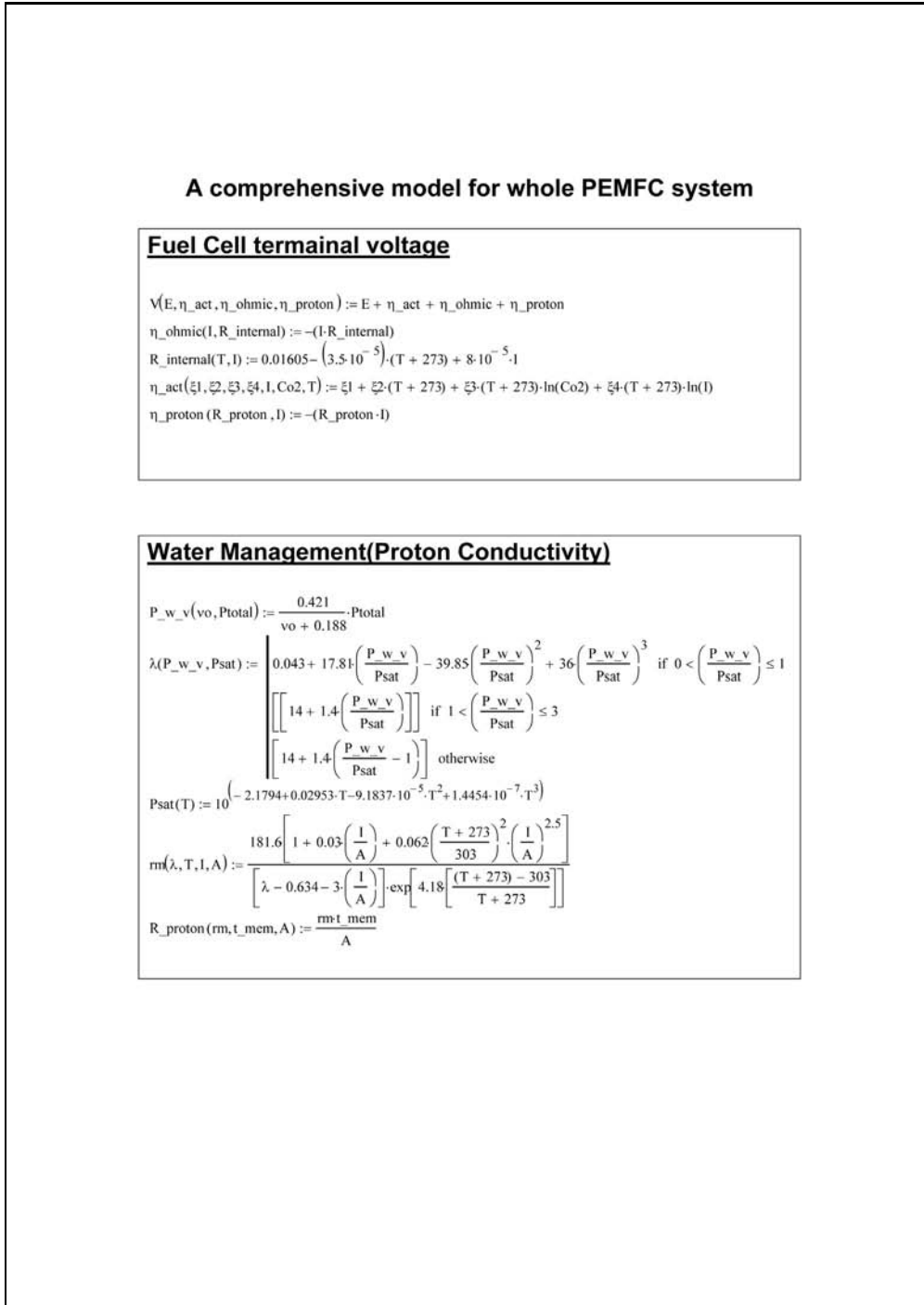


Figure A.1: MatCAD Simulation

Total Energy $P_{total}(Pe, P_{heat}) := Pe + P_{heat}$ **Parameters**

if 40 cell in stack

A := 50.6

 $\xi_1 := -0.944$ $\xi_2 := 0.0035$ $\xi_3 := 7.8 \cdot 10^{-5}$ $\xi_4 := -0.00019$

E := 1

F := 96485

T := 70

 $Mo_2 := 32 \cdot 10^{-3}$ $Mh_2 := 2.02 \cdot 10^{-3}$ $Mair := 28.97 \cdot 10^{-3}$ $Mh_{2o} := 18 \cdot 10^{-3}$ $t_{mem} := 0.0017$ $\eta_{them} := 40$

vo2 := 2

y := 0, 1..3

 $\gamma := 0.21$

cp := 100

 $\gamma_{comp} := 1.4$

T1 := 273 + 30

 $\eta_{comp} := 0.6$

P2 := 2

P1 := 0.8

 $\eta_{ac} := 0.5$ $\eta_{dc} := 0.5$

n := 4C

 $P_{total_0} := 1$ $P_{total_1} := 2$ $P_{total_2} := 4$

Total Energy $P_{total}(Pe, P_{heat}) := Pe + P_{heat}$ **Parameters**

if 40 cell in stack

 $A := 50.6$ $\xi_1 := -0.944$ $\xi_2 := 0.0035$ $\xi_3 := 7.8 \cdot 10^{-5}$ $\xi_4 := -0.00019$ $E := 1$ $F := 96485$ $T := 70$ $Mo_2 := 32 \cdot 10^{-3}$ $Mh_2 := 2.02 \cdot 10^{-3}$ $Mair := 28.97 \cdot 10^{-3}$ $Mh_{2o} := 18 \cdot 10^{-3}$ $t_{mem} := 0.0017$ $\eta_{them} := 40$ $vo_2 := 2$ $y := 0, 1, 3$ $\gamma := 0.21$ $cp := 100$ $\gamma_{comp} := 1.4$ $T_1 := 273 + 30$ $\eta_{comp} := 0.6$ $P_2 := 2$ $P_1 := 0.8$ $\eta_{ac} := 0.5$ $\eta_{dc} := 0.5$ $n := 4C$ $P_{total_0} := 1$ $P_{total_1} := 2$ $P_{total_2} := 4$

```
Ptotal3 := 6  
k := 0..6C  
Ik :=  $\frac{k}{1} + 0.001$   
Psat := Psat(T)  
Psat = 0.307
```

Bibliography

- [1] W.R.Grove, Voltaic Series and the Combination of Gases by Platinum. Phil.Mag. (III) 1838 Vol. 14 p.127.
- [2] W.R.Grove, Gas Voltaic Battery. -Voltaic Action of Phosphorus, Sulphur and Hydrocarbons. Phil. Transactions I 1845 p.351.
- [3] W.T. Grubb, Proceedings of the 11th Annual Battery Research and Development Conference, PSC Publication Committee, Red Bank, NJ, p.5, 1957.
- [4] M.Wakizoe, O.A. Velev, S. Srinivasan, Electrochim. Acta 40 (1995) 335.
- [5] B.Bahar, A.R. Hobson, J.A. Kolde, US Patent No. 5,599,614, 1997.
- [6] Lee J.H., Lalk T.R. "Modelling fuel cell stack systems", Journal of Power Sources, Vol 73, No.2 p.229-241.
- [7] I.D. Raistrick, US Patent No. 48765115, 1989.

- [8] E.A. Ticianelli, C.R. Derouin, A. Redondo, S. Srinivasan, *Journal of Electrochemical Society* Vol. 135, p.2209, 1999.
- [9] T.J. Schmidt, H.A. Gasteiger, R.J. Behm, *Journal of Electrochemical Society*, Vol 146, p.1296, 1999.
- [10] D.P. davies, P.L. Adcock. M. Turpin, S.J. Rowen, *Stainless steel as bipolar plate material for solid polymer fuel cell*, *Journal of Power Sources*, Vol. 86, p.237-242, 2000.
- [11] Hodgson, D.R., *Journal of Power Sources*, Vol 96, p.233, 2001.
- [12] Yang Li, T, *Corrosion resistance PEM fuel cell*, U.S. patent RE37284E, 2001
- [13] Gregor Hoogers, *Fuel Cell Technology Handbook*, CRC press, 2003.
- [14] Zhigang Qi, Arthur Kaufman, *PEM fuel cell stack operated under dry-reactant conditions* *Journal of Power Sources*, Vol. 109, 2002.
- [15] E.Santi, D. Franzoni, A.Monti, D.Patterson, F.Ponci, N.Barry, *A Fuel Cell Based Domestic Uninterruptible Power Supply*, *Applied Power Electronics Conference and Exposition*, Vol.1, 2002.
- [16] A.M. Tuckey, J.N. Krase, *A Low Cost Inverter for Domestic Fuel Cell Application*, *Applied Power Electronics Specialists Conference*, Vol.1, 2002.

- [17] A.Monti, E.Santi, F.Ponci, D.Franzoni, D. Patterson, N.Barry, Fuel Cell Based Domestic Power Supply - A Student Project, Applied Power Electronics Specialists Conference, 2002.
- [18] R.P.Iczkowski, M.B. Cutlip, Journal of Electrochemical Society, Vol. 127 p.1443, 1980.
- [19] S.J.Ridge, R.E. White, Y. Tsou, R.N. Beaver, G.A. Eisman, Journal of Electrochemical Society, Vol. 136, p.1902. 1989.
- [20] T.E. Springer, T.A. Zawodzinski, S. gottesfeld, Journal of Electrochemical Society, Vol. 38, p.2334, 1991.
- [21] M. Eikerling, Yu.I. Kharkats, A.A. Kornyshev, Yu.M. Volkovich, Journal of Electrochemical Society, Vol. 145, p.2684,1998.
- [22] T.V. Nguyen, R.E. White, Journal of Electrochemical Society, Vol.140, P.2178, 1993.
- [23] J.C. Amphlette, M. Farahani, R.F. Mann, B.A. Peppley, P.R. Roberge, Proceeding of 26th Intersociety Energy Conversion Conference, IECEC, p.624-630, 1991.
- [24] A.Cisar, Proceeding of 26th Intersociety Energy Conversion Conference, IECEC, p.611-616, 1991.

- [25] J.Kim, S.Lee, S.Srinivasan,C.E. Chamberlin, Journal of Electrochemical Society, Vol. 142, p.2670, 1995.
- [26] J.H.Lee, T.R. Lalk, A.J. Appleby, Journal of Power Sources Vol 70 p.258, 1998
- [27] J.C. Amphlette, R.M. Baumert, R.F. Mann, B.A. Peppley, and P.R. Roberge, T.J. Harris, Performance Modeling of Ballard Mark IV Solid Polymer Electrolyte Development, Journal of Electrochemical Society, Vol. 42, Jan 1995.
- [28] James Larminie, Andrew Dicks, Fuel Cell System Explained, John Wiley & Sons Ltd., 2000.
- [29] T.A. Zawodzinski, T.E. Springer, S. Gottesfeld, Modeling and experimental diagnostics in polymer electrolyte fuel cells, Journal of Electrochemical Society, Vol. 140, 1993.
- [30] Boca Raton, Handbook of Chemistry and Physics, 62nd ed., CRC Press, 1981.
- [31] Ronald F. Mann, John C. Amphlette, Michael A.I. Hooper, Heidi M. Jensen, Brant A. Peppley, Pierre R. Roberge, Development and application of generalised steady-state electrochemical model for a PEM fuel cell, Journal of Power Sources, Vol. 86, 2000, Page 173-180.

- [32] T.A. Zawodzinski, T.E. Springer, S. Gottesfeld, Polymer Electrolyte Fuel Cell Model, *Journal of Electrochemical Society*, Vol.138, 1991. *Chemical Society*, Vol. 42, Jan 1995.
- [33] T.E. Springer, M.S. Wilson, and S. Gottesfeld, Modeling and Experimental Diagnostics in Polymer Electrolyte Fuel Cell, *Journal of Electrochemical Society*, No. 12, December 1993.
- [34] J.J. Baschuk, Xianguo Li, Modelling of polymer electrolyte membrane fuel cells with variable degrees of water flooding, *Journal of Power Sources*, pp. 181-196, Vol. 86, 2000.